AD-A093 868 SYSTEMS CONTROL INC (VT) PALO ALTO CA F/G 21/5
MULTIVARIABLE CONTROL SYNTHESIS PROGRAM - CONTROL ASPECTS OF TH--ETC(U)
MAR 80 R L DEHOFF, S ROCK, W E HALL F33615-75-C-2053
UNCLASSIFIED AFWAL-TR-80-2010 NL

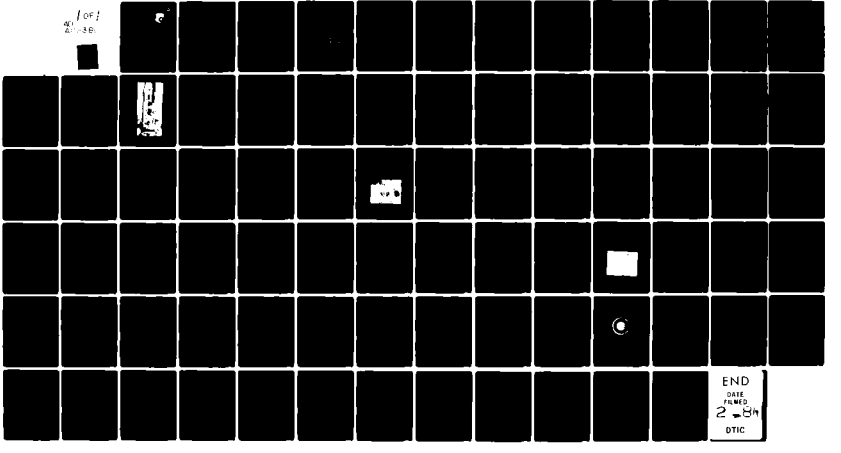

END
DATE FILMED
2-81
DTIC

AFWAL-TR-80-2010

MULTIVARIABLE CONTROL SYNTHESIS PROGRAM — CONTROL ASPECTS OF THE F100 ALTITUDE DEMONSTRATION OF THE MULTIVARIABLE CONTROL SYSTEM

SYSTEMS CONTROL,INC. (Vt)
1801 PAGE MILL ROAD
PALO ALTO, CALIFORNIA 94304

MARCH 1980

TECHNICAL REPORT AFWAL-TR-80-2010
Final Report for Period 1 April 1978 — 31 March 1979

AERO PROPULSION LABORATORY
AIR FORCE WRIGHT AERONAUTICAL LABORATORIES
AIR FORCE SYSTEMS COMMAND
WRIGHT-PATTERSON AIR FORCE BASE, OHIO 45433

NOTICE

When Government drawings, specifications, or other data are used for any purpose other than in connection with a definitely related Government procurement operation, the United States Government thereby incurs no responsibility nor any obligation whatsoever; and the fact that the government may have formulated, furnished, or in any way supplied the said drawings, specifications, or other data, is not to be regarded by implication or otherwise as in any manner licensing the holder or any other person or corporation, or conveying any rights or permission to manufacture, use, or sell any patented invention that may in any way be related thereto.

This report has been reviewed by the Office of Public Affairs (ASD/PA) and is releasable to the National Technical Information Service (NTIS). At NTIS, it will be available to the general public, including foreign nations.

This technical report has been reviewed and is approved for publication.

CHARLES A. SKINA
Project Engineer

DAVID H. QUICK, Lt Col, USAF
Chief, Components Branch

FOR THE COMMANDER

M. I. BUSH
Director
Turbine Engine Division

"If your address has changed, if you wish to be removed from our mailing list, or if the addressee is no longer employed by your organization please notify AFWAL/POTC ,W-PAFB, OH 45433 to help us maintain a current mailing list".

Copies of this report should not be returned unless return is required by security considerations, contractual obligations, or notice on a specific document.

AIR FORCE/56780/14 October 1980 — 130

SECURITY CLASSIFICATION OF THIS PAGE (When Data Entered)

(19) REPORT DOCUMENTATION PAGE	READ INSTRUCTIONS BEFORE COMPLETING FORM
(18) 1. REPORT NUMBER: AFWAL-TR-80-2010	2. GOVT ACCESSION NO.: AD-A093 868
	3. RECIPIENT'S CATALOG NUMBER
(6) 4. TITLE (and Subtitle): MULTIVARIABLE CONTROL SYNTHESIS PROGRAM — CONTROL ASPECTS OF THE F100 ALTITUDE DEMONSTRATION OF THE MULTIVARIABLE CONTROL SYSTEM	(9) 5. TYPE OF REPORT & PERIOD COVERED: FINAL REPORT 1 Apr 1978 — 31 March 1979
	6. PERFORMING ORG. REPORT NUMBER
(10) 7. AUTHOR(s): Ronald L. DeHoff, Stephen Rock, W. Earl Hall, Richard J. Adams	(15) 8. CONTRACT OR GRANT NUMBER(s): F33615-75-C-2053
9. PERFORMING ORGANIZATION NAME AND ADDRESS: SYSTEMS CONTROL, INC. (Vt), 1801 Page Mill Road, Palo Alto, CA 94304	10. PROGRAM ELEMENT, PROJECT, TASK AREA & WORK UNIT NUMBERS: (16) 3066 (17) 03 70
11. CONTROLLING OFFICE NAME AND ADDRESS: AERO PROPULSION LABORATORY, AF Wright Aeronautical Laboratories, AFSC, Wright-Patterson Air Force Base, Ohio 45433	(11) 12. REPORT DATE: March 1980
	13. NUMBER OF PAGES
(12) 83 14. MONITORING AGENCY NAME & ADDRESS (if different from Controlling Office)	15. SECURITY CLASS. (of this report): UNCLASSIFIED
	15a. DECLASSIFICATION/DOWNGRADING SCHEDULE

16. DISTRIBUTION STATEMENT (of this Report)

Approved for Public Release; Distribution Unlimited

17. DISTRIBUTION STATEMENT (of the abstract entered in Block 20, if different from Report)

18. SUPPLEMENTARY NOTES

19. KEY WORDS (Continue on reverse side if necessary and identify by block number)

Modern Control
Optimal Control
Linear Quadratic Regulator Theory
Propulsion Control
Gas Turbine Engine Control
Control System Design
Engine Test

20. ABSTRACT (Continue on reverse side if necessary and identify by block number)

This report describes the engine test demonstration phase of the F100 multivariable control synthesis program. Details of the control system design procedure and results of the hybrid simulation tests are described in AFAPL-TR-77-35, Volumes I and II.

The analytical design of the F100 multivariable control system included a validation of the controller performance using a hybrid simulation. The hybrid simulation represented an "average" F100 turbofan engine and assumed

—next page

DD FORM 1 JAN 73 1473 EDITION OF 1 NOV 65 IS OBSOLETE

SECURITY CLASSIFICATION OF THIS PAGE (When Data Entered)

20. (Continued)

a one-dimensional flow path. Of course, real engine test hardware, which includes the engine, sensing, and control actuator hardware, will behave differently. These differences are recognized by the control designers and, prior to extensive testing at critical design points, these differences and their impact on the controller performance must be quantified.

This report describes the results of the activities to determine the base line engine and sensor/actuator hardware performance. The validation of the engine reference point and trim schedules are included. An analysis of the $\Delta P/P$ (fan exit Mach number) instrumentation, the response characteristics of the basic fuel delivery system, and the contributions due to the response rate of the test facility are presented.

TABLE OF CONTENTS

		Page
I.	INTRODUCTION AND SUMMARY	1
	1.1 Introduction	1
	1.2 Summary	2
II.	F100 MULTIVARIABLE CONTROL STRUCTURE	5
	2.1 Introduction	5
	2.2 Theoretical Synthesis Method	8
	2.3 Functional Description of the Controller	11
	2.3.1 Reference Value Generator	11
	2.3.2 Transition Model	13
	2.3.3 Integral Switching Logic	15
	2.3.4 Engine Protection	18
	2.3.5 FTIT Estimator	19
	2.4 Hybrid Evaluation Results	21
	2.5 Summary	23
III.	OVERVIEW OF F100 ALTITUDE TEST	25
	3.1 Summary of Test Demonstration	25
	3.2 Validation of Reference Point and Trim Schedules	29
	3.2.1 Reference Schedule Correlation	29
	3.2.2 $\Delta p/p$ Instrumentation Evaluation	30
	3.3 Transient Controller Performance	35
	3.3.1 General Response Characteristics	36
	3.3.2 Fuel Valve Anomalies	36
	3.3.3 Test Facility Interaction	39
	3.3.4 Turbine Temperature Limiting	39
	3.4 After-Burner Accommodation	41
	3.5 Summary	44
IV.	SUMMARY AND PERSPECTIVE	45
	4.1 Summary	45
	4.2 A Look at the Future	46
REFERENCES		49
APPENDIX A:	F100 MULTIVARIABLE CONTROL DESIGN RELATED LITERATURE	51

TABLE OF CONTENTS (Continued)

		Page
APPENDIX B:	REFERENCE POINT SCHEDULE EVALUATION	53
APPENDIX C:	ANALYSIS OF $\Delta P/P$ INSTRUMENTATION	59

LIST OF FIGURES

		Page
1.1	F100 MVC Program Team	3
2.1	Typical Mixed Flow/Augmented F100 Engine	7
2.2	F100 Multivariable Control System	11
2.3	Cyclic PLA Transients II at Sea Level Static Conditions from Multivariable Control Digital Evaluation	14
2.4	Operating Envelope Constraint Limits for the F100 Turbofan Engine	16
2.5	Example of Temperature Compensation Showing Compensator Output Leading Both the Actual Temperature Response and Sensor Output During a 75% Thrust Step at 10,000 ft, Mach Number 0.9 from Hybrid Simulation	20
2.6	Computational Setup for Hybrid/Altitude Testing at NASA LeRC	22
3.1	F100 – XD11 Installed at NASA Lewis Research Center Altitude Facility PSL-1	25
3.2	F100 MVCS Altitude Test Point Designation	26
3.3	Area Variation at Constant Speed	31
3.4	Relationship of $\Delta P/P$ to EPR on Fan Map	32
3.5	Comparison of MVC and BOM Bodie Response	37
3.6	Erratic Fuel Valve Behavior	38
3.7	Facility Air Supply/Engine Interaction During Test of MVC Logic	40
3.8	Performance of Updated FTIT Estimator During Snap Acceleration to Temperature Limited Condition (MVC Engine Test -- Alt = 10K, Mn = 0.6)	42
3.9	Afterburner of F100 Engine	43
3.10	Afterburner Supression Curve	44

LIST OF TABLES

		Page
3.1	Summary of F100 MVCS Hybrid Evaluation and Altitude Test Conditions	26
3.2	Station Location for $\Delta p/p$ Synthesis	34
3.3	F100 (XD11) Fan Exit $\Delta p/p$ Instrumentation Recommendation	34

CHAPTER I
INTRODUCTION AND SUMMARY

1.1 INTRODUCTION

Aircraft missions of the next decade and beyond are dictating the requirement for multimode integration of airframe and propulsion systems over wide operational envelopes. Aircraft engines have accordingly become more sophisticated in the evolutionary design process which must eventually meet these future requirements.

The provision for multimode propulsion response, without sacrificing efficiency or performance, is achievable by engines with variable geometry. Such engines are controlled by commanded internal geometrical changes. This capability is achieved at the expense of a significant increase in engine complexity, addition of actuators, and sensors. The subsequent control system requirement to maintain strict transient and steady-state performance specifications forces attention to more accurate and reliable controller implementations. Evaluation of engine control technology has demonstrated that such functions should be implemented with digital multivariable designs, relying on hydromechanical hardware for back-up, fail/operate functions. Control synthesis techniques for such digital systems must therefore be developed and demonstrated to fill the need for accurate response, high reliability, and compatibility with state-of-the-art digital processing capability.

One potential control design technique for achieving these objectives is based on quadratic synthesis methods. These are usually identified as modern control, optimal control, linear-quadratic-Gaussian (LQG), or linear-quadratic-regulator (LQR) methods. They have undergone extensive

theoretical development. The results have indicated that they can serve as the basis for a systematic, comprehensive procedure to design practical multivariable digital controllers to satisfy complex engine performance requirements.

To evaluate the potential benefits of these multivariable design methods, the Air Force Aero-Propulsion Laboratory and the NASA Lewis Research Center have cooperatively sponsored a comprehensive research and development program of an advanced multivariable controller for the F100 turbofan engine. The objective of this program is specifically to design and demonstrate a practical multivariable controller for the F100 over its operating envelope. The design methodology is to be based on LQR control methods, and the controller performance evaluated on a detailed nonlinear digital simulation, a hybrid simulation, and on tests of an actual F100 engine. To accomplish this objective, the AFAPL and NASA-LeRC contracted for the controller design to Systems Control, Inc. (Vt) and, for the F100 engine technology expertise, to Pratt & Whitney Aircraft Group, Government Products Division. The overall agency integration is illustrated in Figure 1.1.

1.2 SUMMARY

The report describes the F100 multivariable controller altitude test demonstration. In particular, the impact of a hardware implementation on the control design is addressed. The report focuses on several topics which evolved during the phase II test activity in detail. The altitude cell tests results themselves are presented in the NASA-LeRC phase II evaluation report [1]. The controller synthesis methodology and design description is the subject of Ref. [2]. Additional material describing the control development and hybrid evaluation is contained in Refs. 3 and 4.

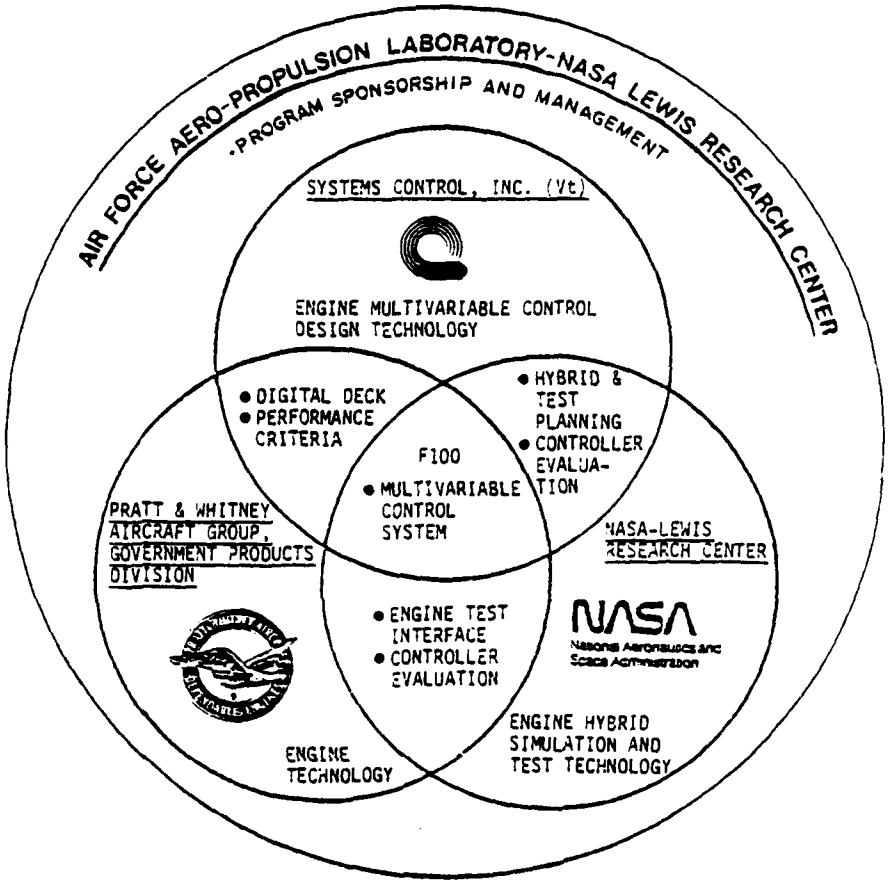

Figure 1.1 F100 MVC Program Team

This report is organized as follows:

- Chapter II – F100 Multivariable Control Structure

  The MVCS design is reviewed. Controller functions are described and the interconnection of control modules is treated. Design synthesis methods for each block are referenced. Hybrid test results are summarized.

- Chapter III – Overview of Altitude Test Demonstration

  The MVCS evaluation in the NASA-LeRC test cell is reviewed. Major results are presented. Specific topics are described including (1) reference schedule evaluation, (2) $\Delta p/p$ data analysis, (3) transient performance, and (4) afterburner accommodation.

- Chapter IV – Summary and Conclusion

  The F100 MVC design program is reviewed. Major milestones in the design and evaluation of the controller are described. Conclusions regarding the synthesis approach and future system concepts are included.

- Appendices

  The appendices include the specific test data evaluations performed during the Phase II MVCS test demonstration.

CHAPTER II

F100 MULTIVARIABLE CONTROL STRUCTURE

The F100 multivariable control system (MVCS) is reviewed. Appendix A contains a complete bibliography of the literature relevant to the various aspects of this comprehensive development and demonstration program. This material is included to provide background information essential to an appreciation of the test results described in the subsequent sections. The MVCS design is completely treated in Ref 2.

2.1 INTRODUCTION

Over the past several years, aircraft operational requirements have dictated the development of propulsion systems having increased performance over a wider operating envelope. To satisfy these performance requirements, variable geometry components have become an integral part of advanced aircraft engines. Future variable cycle engines may incorporate variable fan, compressor, turbine and exhaust nozzle geometry to improve overall performance [1]. As a result, the engine control system will have to be capable of controlling engine fuel flows and the variable geometry in an "optimum" manner. This will necessitate the measurement of more engine variables. However, the multitude of variables to be manipulated and measurements to be utilized make it difficult to design controls for these advanced engines.

Classical control synthesis techniques, which involve the analysis and design of single-input, single-output control loops, have worked quite well for the older, simpler engines. Unfortunately, such techniques prove to be cumbersome and time-consuming when they are applied to the more complex multivariable engines.

One approach to solving the engine control problem is the use of multivariable (optimal) control theory. The LQR is one aspect of the theory that has been successfully developed and applied to a wide variety of linear multivariable control problems [2]. LQR designs result in feedback-type controllers which make use of inherent loop interactions to improve performance. The LQR control modes can also reduce the sensitivity to parameter variations and sensor inaccuracies.

The F100 (see Figure 2.1) engine was selected for the MVCS program due to the availability of detailed digital and hybrid computer simulations of that engine and the availability of an actual F100 engine for testing at NASA Lewis Research Center. The F100 engine represents the current state-of-the-art in aircraft gas turbine technology. Although not as complex as some of the advanced cycles being proposed, the F100 does provide a suitable test for the LQR technique. In addition to the main burner and afterburner fuel flows, the F100 has variable fan inlet guide vanes, variable compressor stator vanes and a variable convergent-divergent exhaust nozzle. Airflow bleed can be extracted at the compressor exit.

Certain restrictions were placed on the control design. The design approach would use linear engine models as a basis for the control synthesis. Deterministic LQR theory was to be applied exclusively, i.e., as a first approximation, the random uncertainty associated with the engine behavior was assumed to be negligible. Only existing sensed variables were to be used as control inputs. The controller authority was to include engine operation from idle to max dry power. Start-up and afterburner regimes were excluded; however, during the hybrid simulation and engine tests, afterburner lights were done to assess the controller's regulation capability in the presence of disturbances.

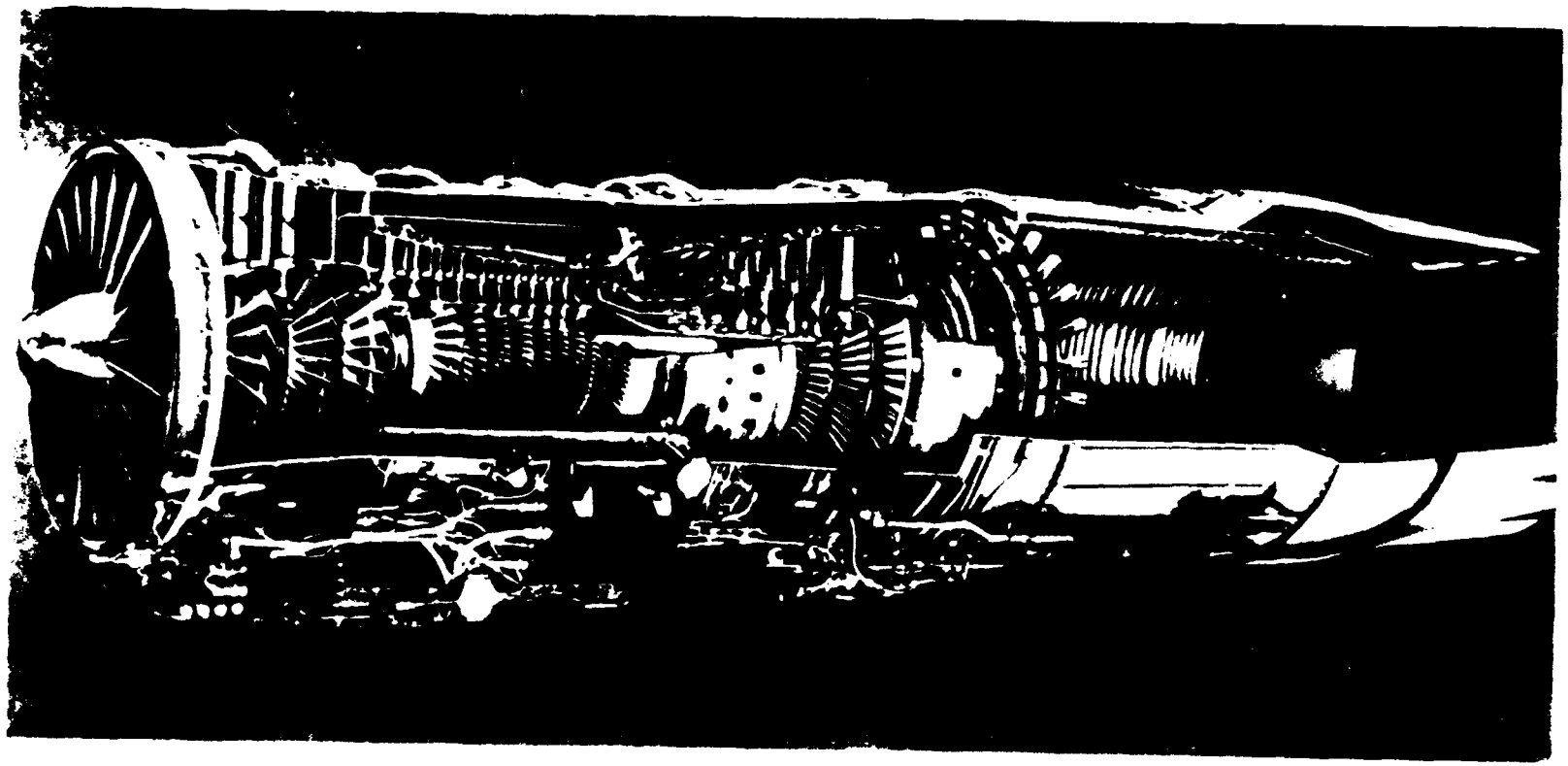

Figure 2.1 Typical Mixed Flow/Augmented F100 Engine

Prior to the actual control design, detailed criteria were established that specified the desired engine performance [3]. The control criteria can be summarized as follows. Foremost, the control must protect the engine against surge and from exceeding speed, temperature and pressure limits. Airframe-engine-inlet compatibility requirements specify minimum burner pressure limits and maximum and minimum airflow limits at certain flight conditions. The control must insure engine thrust and fuel consumption are within tolerance for specified engine degradations and for installation effects. The engine must also accelerate and decelerate smoothly, safely, quickly and repeatably with small overshoots allowable. It must do this for both large and small requested power level movements and during flight maneuvers.

2.2 THEORETICAL SYNTHESIS METHOD

The fundamental aspects of locally linear control synthesis are reviewed as applied to the synthesis of the control and the fundamental requirements of the control structure. The engine may be modeled conceptually as a nonlinear time-invariant dynamical system utilizing fundamental aerodynamic principles as follows:

$$\dot{x} = f(x,u,\theta) \tag{2.1}$$

$$\dot{y} = h(x,u,\theta) \tag{2.2}$$

where n states, x, m controls, u,p outputs, y, and a q parametric variables θ, as well as the detailed nonlinear dynamics $f(x,u,\theta)$ and measurements $h(x,u,\theta)$, are modeled by the designer to achieve his purpose most expediently. For engine development, detailed digital simulations, including thorough component maps and experimentally correlated gas path equations, are utilized as in the F100 transient simulation deck. These programs are too complex for control synthesis, but are useful in evaluating a candidate design.

Locally linear models can be generated from nonlinear simulations or experimentally from engine data via system identification. These models are valid in the neighborhood of an equilibrium point (x_o, u_o, θ_o) and describe perturbation motion $\delta x, \delta u$, away from equilibrium. These models are represented as follows:

$$\delta\dot{x} = F\delta x + G\delta u \tag{2.3}$$

$$\delta y = H\delta x + D\delta u \tag{2.4}$$

where, in principle,

$$F = \frac{\delta f(x, u_o, \theta_o)}{\delta x}\, x=x_o \tag{2.5}$$

δx and δu will be rewritten as x, u in the remainder of this paper.

Model reduction procedures can be utilized to produce linearized equations containing convenient, control oriented parameters. The reduction was performed on the linear system equations in each region of the operating envelope to provide a set of models used in the optimal regulator synthesis. The total procedure to arrive most efficiently at multivariable designs requires the utilization of a blend of techniques incorporating frequency and time domain analysis and modern and classical control concepts.

Given the linear design model (Eq. (2.3)), and the state/control performance index,

$$J = \frac{1}{2}\int_o^\infty (x^T Ax + u^T Bu)dt \tag{2.6}$$

or the output performance index,

$$J = \frac{1}{2}\int_o^\infty (y^T A^* y)dt \tag{2.7}$$

the deterministic, steady-state optimal controller to minimize J for arbitrary initial conditions about a fixed set point

is given by the following state variable regulator control law:

$$u = u_o + C(x - x_o) \tag{2.8}$$

$$C = -B^{-1}G^TS \tag{2.9}$$

where u, x are a consistent equilibrium reference point for the nonlinear plant, namely,

$$0 = f(x_o, u_o) \tag{2.10}$$

where f[x(t),u(t)] describes the nonlinear engine behavior exactly. The matrix S is given by the positive definite solution of the algebraic Ricatti equation (for Eq. 2.6).

$$0 = SF + F^TS + A - SGB^{-1}\ G^TS \tag{2.11}$$

and by a comparable form for Eq.(2.7). The solution is calculated numerically by integration of the matrix Ricatti differential equation to steady-state or, more efficiently, by the eigenvector decomposition method. The optimality of such regulators is given in terms of a fixed set point. However, with reasonable choices of weighting parameters, system response is not degraded for varying set-point inputs.

The state or output weightings can be constructed initially from physical reasoning. Alternately, if it is desired to alter the dynamic response in terms of time domain specifications (e.g., rise time or damping), state weightings on the variables most nearly associated with the mode to be controlled are chosen. State variables and output quantities often are related physically. Control of the state is then equivalent to control of the output. In this case, the need for explicit output weighting is removed. For example, engine thrust, an output and augmentor pressure, a state, have nearly the same coefficient representation. Thus, weighting P_{T6} results in direct control of thrust response. Such considerations can give the designer a foundation for the initial quadratic weighting matrix selection.

2.3 FUNCTIONAL DESCRIPTION OF THE CONTROLLER

Figure 2.2 shows a schematic representation of the digital controller. The control structure is applicable to many physical, nonlinear systems with state, control and output constraints. Each functional component of the system produces an element of the control law. The multivariable control law is expressed by Eq. (2.12).

$$u = u_s + C_x(x - x_s) + \int C_y A(y - y_s)dt \qquad (2.12)$$

The feedback law itself represents an optimal structure with integral trims for steady-state accuracy and a model following implementation to prevent saturation during transients.

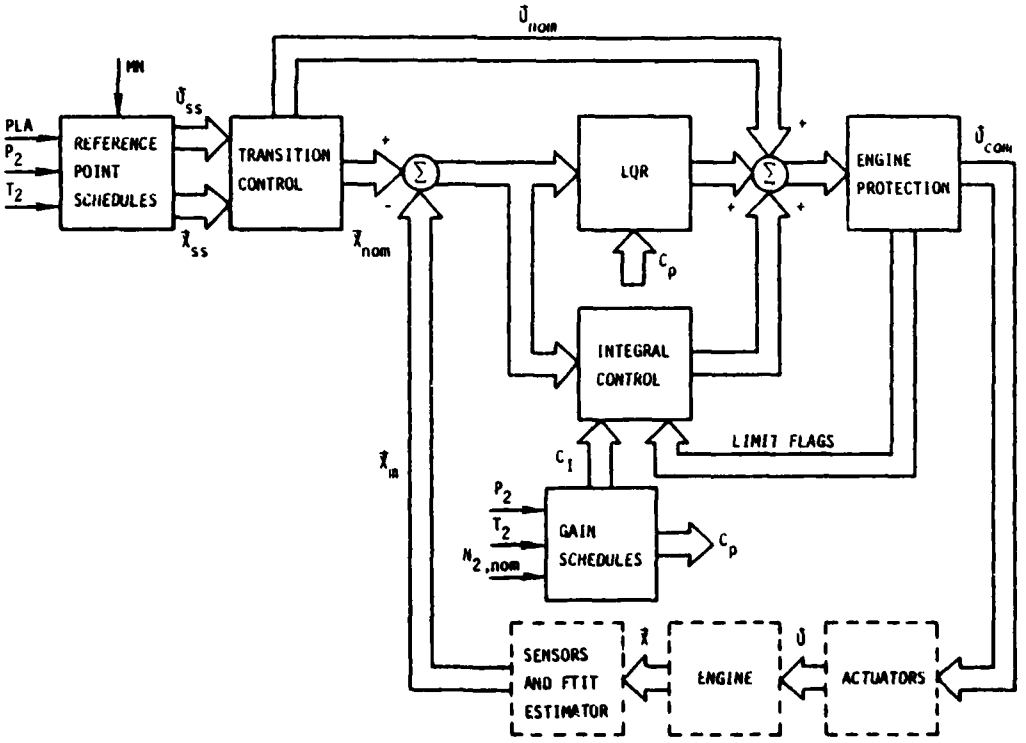

Figure 2.2 F100 Multivariable Control System

Each element of the control law will be described relative to the F100 implementation, and the synthesis procedure for each block will be reviewed briefly.

2.3.1 Reference Value Generator

The control law is written for state and control perturbations about an equilibrium condition. The equilibrium conditions must be derived approximately by the controller given the requested power level, altitude, Mach number, engine face pressure and temperature. Because of manufacturing tolerances and engine aging, an exact expression for these quantities is not possible. Inaccuracies in the scheduled reference values normally would cause steady-state "hang-offs" unless compensated with an integral trim action. Small inaccuracies do not degrade transient performance, and indeed, the feedforward structure allows lower regulator feedback gains and the associated model parameter insensitivity of the control.

The reference schedules are produced by calculating the thermodynamic equilibrium associated with a given control vector. The manufacturer-specified steady-state condition requires zero bleed flow and scheduled compressor geometry. Two degrees of freedom are left to attain desired thrust (power level) at a particular flight point. The reference point generator attempts to set a fan matchpoint to achieve equilibrium. The current control mode is to specify the fan matchpoint using fan rotor speed and fan exit Mach number ($\Delta p/p$).

A representative group of subsonic and supersonic flight points was chosen, and the engine equilibrium points were calculated. Nondimensionalized quantities were utilized to fit approximate reference points with minimum complexity. The regulator is tolerant of the schedule errors and produces

smooth transient responses without an overly complex implementation.

2.3.2 Transition Model

When a large transition in power is requested by the pilot, the perturbation character assumed in the regulator design is lost. A large change in the reference state vector will cause large commanded inputs, tending to saturate actuators and produce significantly nonlinear behavior. The regulator can be used to track a compatible trajectory taking the system for one state to another. Exact calculation of such trajectories is complex, and their practical implementation has not been investigated. A first-order approximation to an achievable state trajectory can be calculated directly from the linearized models [2].

In the F100 implementation, rates were calculated for low, middle and high power. In the latter two cases, desired thrust and turbine inlet temperature rates characteristic of the engine were chosen. At low power, thrust and either burner pressure or surge margin rates were specified, depending on the flight condition, in order to specify adequate acceleration surge margin or eliminate burner pressure undershoot. Figure 2.3 shows the response of the nonlinear digital simulation to a large-power-level modulation. Engine state and trajectory time histories are shown, along with error terms in the regulator portion of the control law. The transition model prevents large error terms from saturating actuators during gross transients while still providing stiff regulation near steady-state conditions. The implementation of this type of transition algorithm requires very little control logic and storage. The performance is excellent and the processing overhead is minimal.

The dynamic response of the engine is affected strongly by the air mass flow. Power level, altitude and Mach number

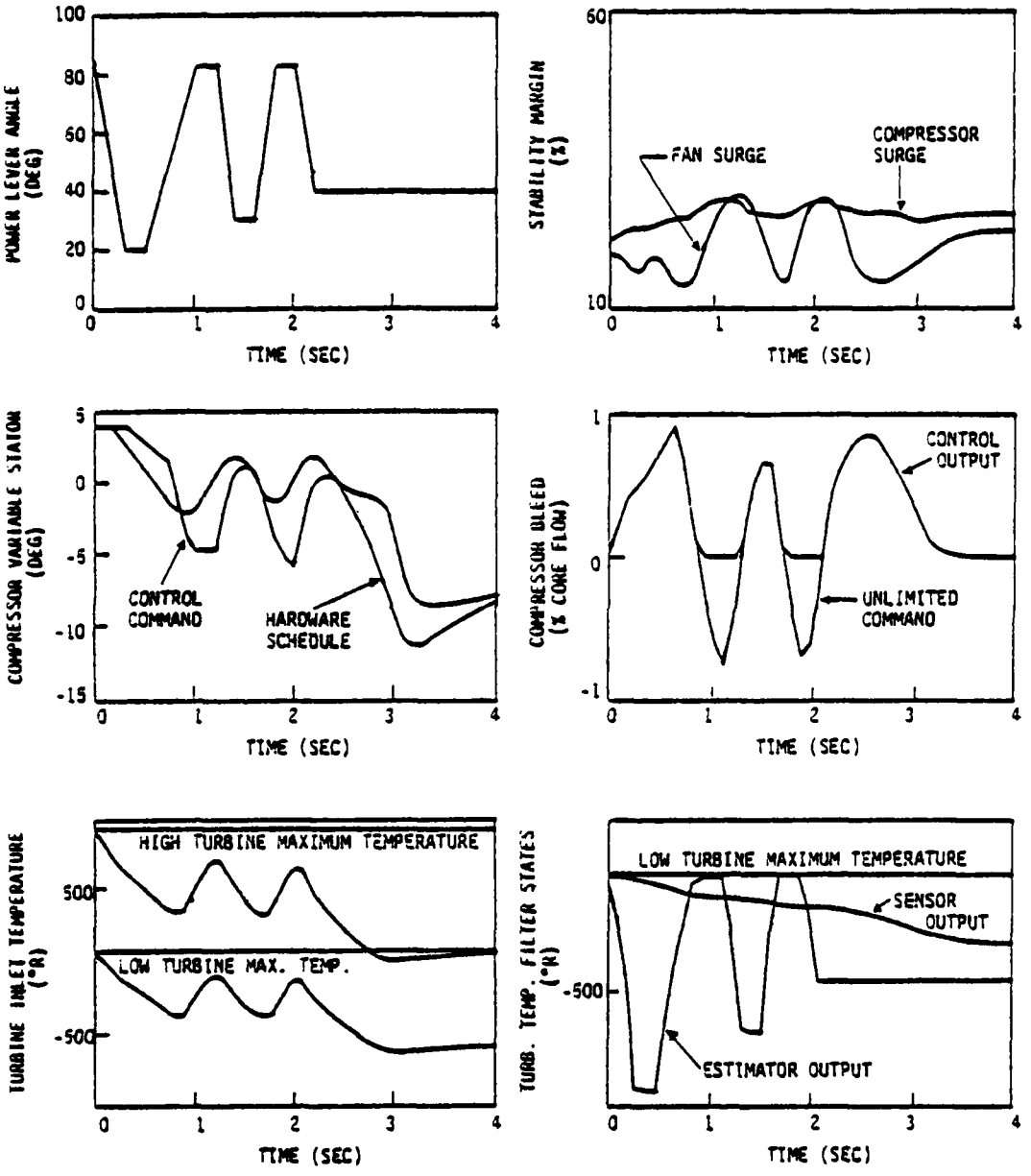

Figure 2.3 Cyclic PLA Transients II at Sea Level Static Conditions from Multivariable Control Digital Evaluation

determine this mass flow and the response. The linearized control synthesis (LQR) procedure produces regulator gains that control the engine satisfactorily in the neighborhood of the design flight/power point. To implement a continuous envelope-wide controller, the gains must be varied as the system makes the transition from one condition to another.

There is no precise analytical relationship between gains at neighboring linearization points. Although engine time constants can be modeled as functions of the ambient conditions, the performance index is chosen by the designer to satisfy specifications particular to the flight point. For example, a function of ambient variables will not correlate exactly the gain elements between sea level static idle conditions, where thrust stability is weighted heavily, and subsonic altitude idle, where burner pressure is the dominant state weight. The procedure adopted for the F100 implementation approximately fit important gain elements with univariate functions of the engine face density and rotor speed. The former variable accounts for altitude effects, while the latter schedules the power condition. Dominant gain elements are determined by assessing the closed-loop eigenvalue sensitivity of the system to each gain element and eliminating those that do not affect closed-loop response. Over 50 percent of the scheduled control gains, C_x and C_y, were elminated in the final implementation with little or no effect on system performance.

2.3.3 Integral Switching Logic

The design philosophy of aircraft turbine engines dictates that steady-state performance is obtained at various flight conditions when a particular physical limit is held exactly (see Figure 2.4). For example, sea level static take off thrust for the F100 is defined as the thrust obtained at the maximum allowable turbine inlet temperature. At

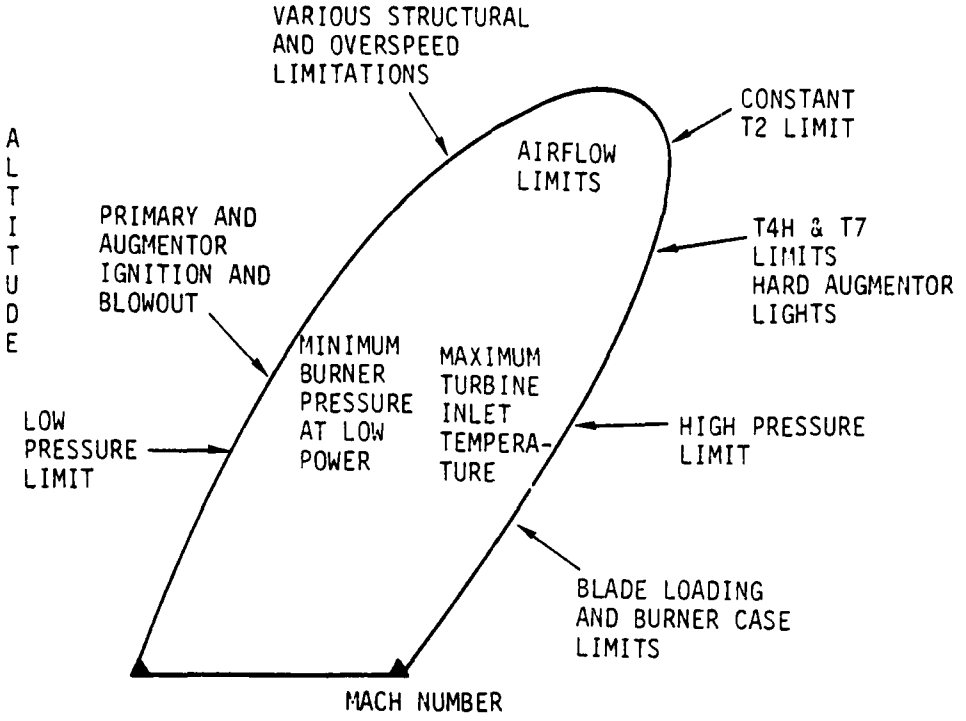

Figure 2.4 Operating Envelope Constraint Limits for the F100 Turbofan Engine

lower power levels, the engine operation should cause the airflow and low rotor speed to attain predetermined values for optimum efficiency. At altitude conditions, the minimum burner pressure defines engine idle. Inlet airflow requirements and burner burst pressure determine operating conditions at some supersonic flight points.

The engine set-point is a group of reference values of states and controls which the engine must attain exactly in steady-state. These values define the equilibrium point. Since the F100 has set-point vectors whose elements change with flight and power conditions, a switching structure from trim control is required.

Given the design model (Eq. 2.3) and the linear quadratic regulator design (Eq. 2.8), the closed-loop response to additive control inputs may be written as follows:

$$\dot{x} = (F + GC_x)\, x + Gu' \tag{2.13}$$

where

$$u = C_x x + u' \tag{2.14}$$

and u' is the additional control input. If the trim responses (i.e., the integral control time constants) are decoupled spectrally from the transient equations, i.e., time constants of Eq. 2.13, then the following should be approximately valid:

$$\dot{x} = 0 \tag{2.15}$$

$$x = -(F + GCx)^{-1} Gu' \tag{2.16}$$

$$y = [\, -(H + DC_x)(F + GC_x)^{-1} G + D]\, u' \tag{2.17}$$

or, $$y = H^* u' \tag{2.18}$$

The output vector y is chosen as m quantities, which must be held in steady-state to their reference values. (Controllability is assured, then, if H^* is invertible.) The trim integrations provide system dynamics, namely,

$$\dot{b} = y \tag{2.19}$$

The control law is designed:

$$u' = C_y b \tag{2.20}$$

and the full controller is implemented:

$$u = C_x x + \int C_y y\, dt \tag{2.21}$$

where elements of y and C_y can be switched arbitrarily while maintaining a continuous control time history.

Design methods produce a single m x r gain matrix, where r is the total number of possible output quantities. If ℓ controls are saturated, m-ℓ elements of the r output quantities can be chosen for trim. The control law then is

implemented as in Eq.(2.21), with the ℓ rows corresponding to the saturated actuators deleted from the matrix. The control is switched when an actuator saturates (delete a row and column), an engine limit must be accommodated (a column is replaced), or the error term associated with the saturated control will tend to unsaturate the control (add the row and column). The implementation produces an extremely simple structure for trim and transient control action which can accommodate various engine limits and control saturations, as well as obtain rated engine performance accurately throughout the flight envelope. Three elements of the set-point vector are the vane, stator and bleed schedules. These error terms always are integrated unless they are driven transiently into saturation. To avoid integrator wind-up due to this uncontrollable situation, the appropriate error is switched out until the transient command tends to cause the control to unsaturate. The remaining two elements of the set-point are normally, scheduled low rotor speed and an averaged fan exit total to static pressure difference $\Delta p/p$. The $\Delta p/p$ error term is elminated if the jet area saturates. If burner pressure or turbine inlet temperature limits are reached, these terms are substituted for low rotor speed in the control law. The switching logic provides smooth and controlled engine transitions in power and flight condition.

2.3.4 Engine Protection

The engine protection logic in the multivariable control provides hard limits on the commands to the control actuators. The engine protection logic includes fuel flow limits, variable vane limits, bleed air limits and exhaust nozzle area limits. The fuel flow limits include the maximum and minimum fuel flow and an acceleration schedule, which is

a function of measured compressor speed. Axial and cambered limits are imposed on the variable vane position. The maximum and minimum nozzle area limits are scheduled as a function of power lever angle. The maximum and minimum allowable area commands converge at idle power so as to prevent limit cycling in this operating region. Whenever a commanded actuator position exceeds a specified limit or when a control saturation is detected, a flag is set within the control logic. These flags send a signal within the logic to clamp and hold the appropriate trim integrator to prevent integrator wind-up.

2.3.5 FTIT Estimator

As specified by the manufacturer, temperature limiting during transient and steady-state operation is a critical function of any turbine engine control system [3]. For the F100, the maximum temperatures specified for compressor discharge and turbine inlet stations in the gas path are implicitly limited by region, then, is absolutely necessary for successful engine control. Unfortunately, the FTIT sensor output response is extremely slow relative to the temperature overshoot criteria. Compensation of this signal is required for adequate temperature limiting during transient maneuvers. The compensation technique must not degrade the high d.c. accuracy of the signal because this measurement sets intermediate thrust at a majority of flight points.

A steady-state, third-order filter was designed. The FTIT "estimator" uses a combination of the sensed FTIT, the steady-state reference value of FTIT, the transition value of fuel flow and the commanded fuel flow to predict the final value of FTIT during a transient. The predicted FTIT is then compared to the maximum allowable FTIT. If the

overtemperature is predicted, the fuel flow integrator begins downtrimming fuel flow before an actual overtemperature can occur.

The FTIT sensor output is attenuated at high frequencies within the filter. The steady-state gain of the estimator to the sensed input is nearly unity, preserving the high d.c. accuracy of the measurement. The two fuel inputs are used to provide the initial high frequency response compensation of the sensed temperature. The estimator functions as a complementary filter in blending inputs of two types to form a system with acceptable response and accuracy.

An example of the performance of the estimator is shown in Figure 2.5. The overshoot occurs in advance of the actual FTIT response. This enables the controller to use the estimator output to modulate the controls to reduce

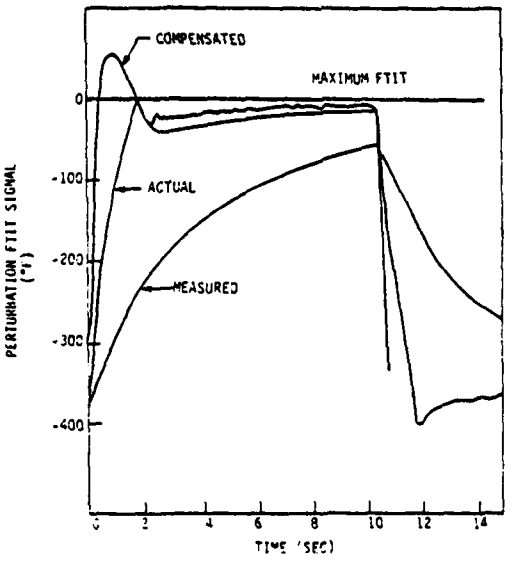

Figure 2.5 Example of Temperature Compensation Showing Compensator Output Leading Both the Actual Temperature Response and Sensor Output During a 75% Thrust Step at 10,000 ft, Mach Number 0.9 from Hybrid Simulation

actual temperature overshoots. Whenever an acceleration occurs that will not cause a temperature limit to be exceeded, the estimator output is not used to throttle back fuel flow. Thus, off-intermediate power accelerations are not penalized by the temperature limiting logic.

2.4 HYBRID EVALUATION RESULTS

Initially, the control logic was validated on the F100 digital simulation. During these tests, small transient responses were run to verify the steady-state regulatory performance. Large power lever transients were run to test the limit protection logic and the transition controller. Disturbances were generated to investigate the effects of augmentor ignition and inlet distortion. Utilizing the unique flexibility offered by the digital simulation, accelerations at sea level static conditions with severe engine deterioration and power extractions were done to test the control in this critical region. The digital evaluation provided a preliminary test of the logic at a limited set of flight conditions to validate the design and structure of the control logic.

The F100 multivariable control logic was then implemented on a SEL810B digital computer and evaluated on a hybrid computer simulation of the F100 engine at the NASA Lewis Research Center. The SEL810B is a general purpose computer processor, and although not flight qualified hardware, its memory, speed and word size are believed to be representative of computers that will be used to control engines in the 1980's. Figure 2.6 is a schematic of the hybrid system. The primary objective of the hybrid evaluation was to verify the multivariable control logic and its implementation to ensure safe and stable operation of the F100 engine during subsequent altitude tests. The results of the evaluation indicated that the control logic and its implementation will

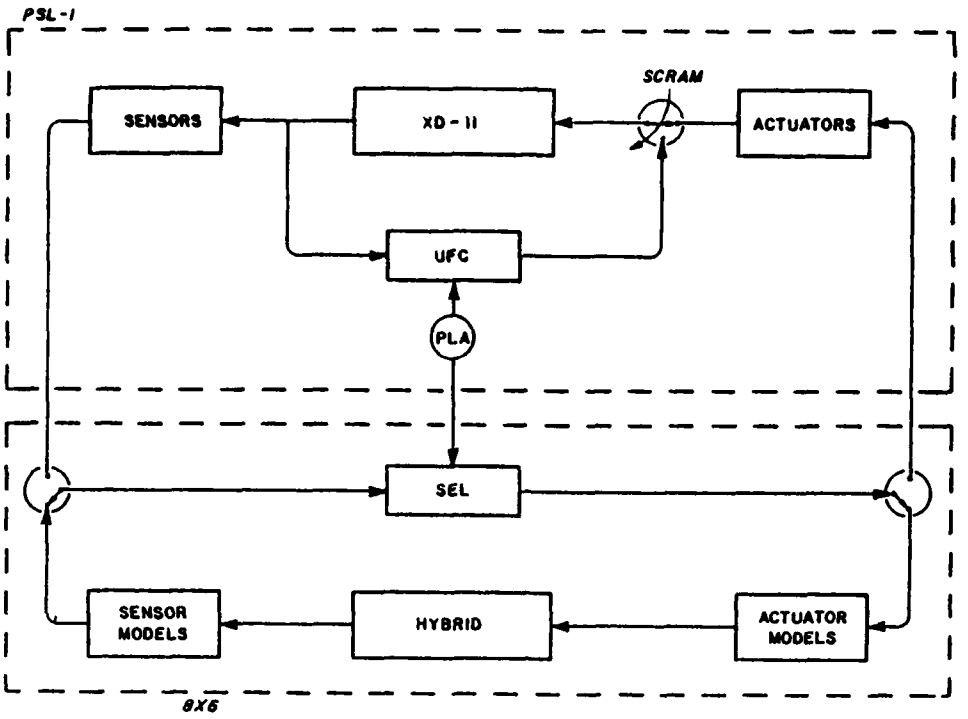

Figure 2.6 Computational Setup for Hybrid/Altitude Testing at NASA LeRC

be capable of controlling the engine throughout its operating range. The specified engine limits were not violated during normal steady-state and transient operation.

In all, 56 steady-state operating points were recorded and 77 transient tests were performed during the hybrid evaluation.

The multivariable control matched baseline, steady-state performance for all but a few supersonic test conditions. The degraded supersonic performance was attributed to reference point scheduling errors at those conditions. Minor modifications to the reference point schedules will produce satisfactory steady-state performance at all flight conditions. The proportional (LQR) plus integral control structure provided good fan operating point control and when required, tracked the engine limits.

The LQR and transition control produced satisfactory transient responses at most operating conditions. The specified response time requirements were satisfied for all small and large amplitude transients with the exception of the small (+3°) PLA snaps at the sea level/static, idle condition. A 1.2 second response time requirement for the small perturbations was adopted due to a lack of specificity in the design criteria.

The results of the sensor failure study at the 30,000ft/ 0.9 condition indicated that most sensor failures would result in a safe, downtrimming to a part-power condition. The saturation of the PT2 sensor or the loss of the fan speed sensor, however, resulted in an overspeed and over-temperature condition.

Therefore, a simplified sensor failure detection logic was implemented in the multivariable control prior to engine testing. MAX, MIN and delta checks were made against each sensor. These limits were determined using data gathered during the hybrid evaluation. Three consecutive "failure" conditions indicated a failed sensor. For noncritical sensors, the value from the reference point schedule was used instead of the failed channel. For failed PT2 and fan speed signals, the MVCS logic was disengaged and the engine power was cut back to a safe level.

Based on recommendations from NASA Lewis Research Center and from Pratt & Whitney engineers, the MVCS control logic was approved for engine test demonstration at NASA Lewis Research Center.

2.5 SUMMARY

The objective of the F100 Multivariable Control Synthesis Program was to demonstrate that a control could be designed

using LQR design methods that would operate a modern turbofan engine over its entire flight envelope. The LQR design methods were used to develop feedback gains for a series of operating points. Reference schedules were used to translate pilot and ambient inputs to reference point specifications. A transition controller was used to produce smooth and rapid transitions from one operating point to another. A variable structure integral trim control was designed to produce specified steady-state performance and to accommodate limits. The performance of the multivariable control was evaluated on a real-time simulation of the P&W F100 turbofan engine with the control logic programmed on a digital computer. Use of the real-time simulation allowed program debugging and verification of proper control logic functioning prior to engine tests in an altitude facility. Sensor and actuator failure detection logic was developed and checked out by simulating transfers from multivariable to a backup control.

CHAPTER III

OVERVIEW OF F100 ALTITUDE TEST

3.1 SUMMARY OF TEST DEMONSTRATION

The F100 engine, XD11, was installed in the NASA LeRC test cell, PSL-1, and instrumented for MVCS application [1] (see Figure 3.1).

Engine tests were run at five subsonic and four supersonic test points (see Figure 3.2). The flight conditions and the types of tests conducted are shown in Table 3.1. In certain regions, air flow and burner pressure constraints limit the

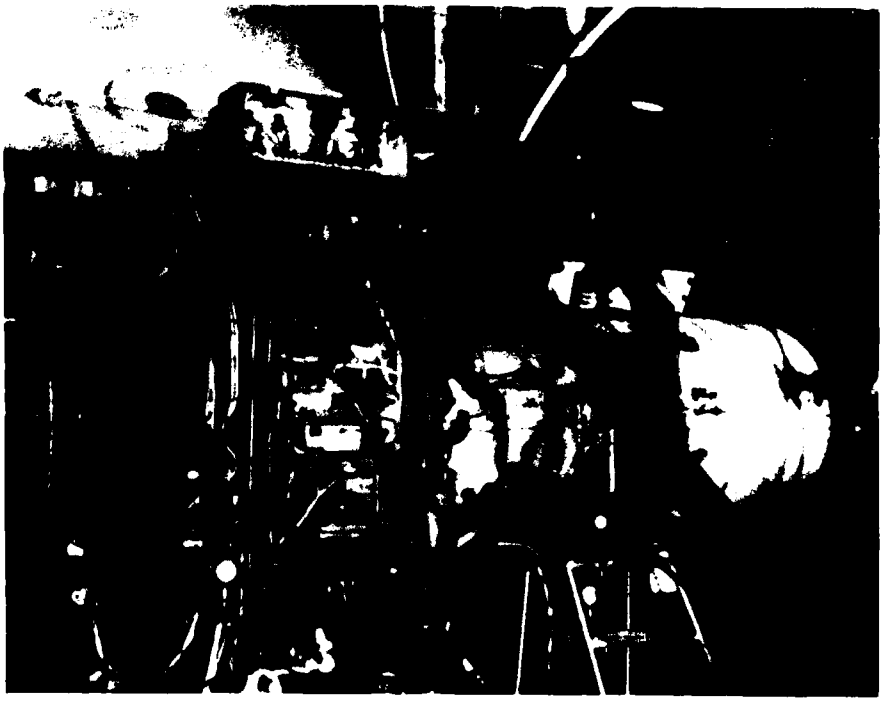

Figure 3.1 F100 – XD11 Installed at NASA Lewis Research Center Altitude Facility PSL-1

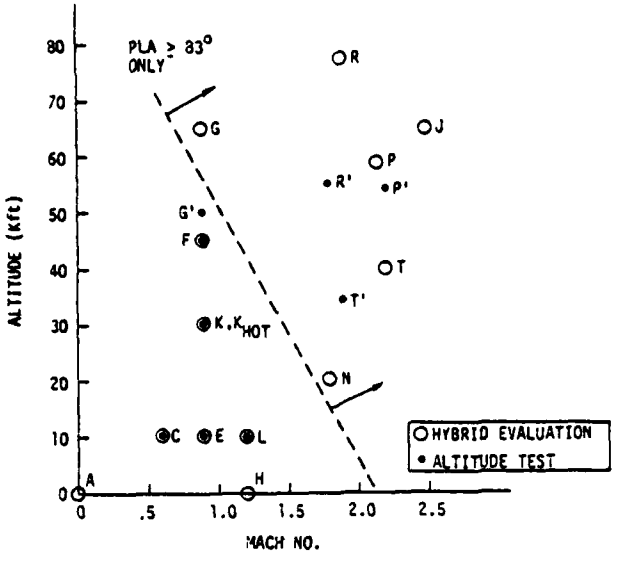

Figure 3.2 F100 MVCS Altitude Test Point Designation

Table 3.1

Summary of F100 MVCS Hybrid Evaluation and Altitude Test Conditions

ALTITUDE (FT) MACH NUMBER	STEADY STATE		POWER LEVER ANGLE PLA TRANSIENTS			DISTURBANCES		SENSOR FAILURES
	PLA = 83°	PLA < 83°	LARGE	SMALL	CYCLIC	AFTER-BURNER	MANEUVER OR FAST ACCEL	
0/0	●	●	●	●	●	●	●	
10/0.6	● ▲	● ▲	● ▲	● ▲	● ▲	● ▲	● ▲	
10/0.9	● ▲	● ▲	● ▲	● ▲	● ▲	● ▲	● ▲	▲
30/0.9	● ▲	● ▲	● ▲	● ▲	● ▲	● ▲	● ▲	
45/0.9	● ▲	● ▲	● ▲	● ▲	●	● ▲	●	●
50/0.9	● ▲	● ▲	● ▲	● ▲	●	● ▲	●	
65/0.9	●					●	●	
0/1.2	●	●	●	●		●	●	
10/1.2	● ▲	● ▲	● ▲	● ▲		●	●	
20/1.8	●					●	●	
55/1.8	▲					▲		
35/1.9	▲					▲		
75/1.9	●					●	●	
40/2.2	●					●		
55/2.2	▲					▲		
60/2.15	●					●	●	
65/2.3	●					●	●	

● HYBRID TEST

▲ ENGINE TEST

range of steady-state operation to near intermediate (PLA = 83°) operation. Transient control performance was evaluated by subjecting the control to small (3°) PLA steps, to large PLA snaps and chops, to random, cyclic PLA motion and to zone one afterburner lights. In addition, simulated flight maneuvers were performed during the engine tests.

Prior to the MVCS tests, over 225 steady-state and 91 transient tests were recorded using the standard F100 control logic. These baseline tests were performed to record the XD11 engine's reference point values. Also, total and static pressure data at station 2.5 were recorded and used to synthesize the fan discharge $\Delta p/p$ parameters.

From these tests, it was found that engine XD11 differed significantly in operating characteristics from the nominal engine described by the digital simulation. Since the reference point schedules used in the MVCS control were based on simulation data, some adjustments were made to the reference point schedules prior to engine test. Also during the baseline tests, the MVCS limit mode switching logic and failure detection logic were thoroughly checked out.

Steady-state operating data were taken at 309 combinations of flight condition and power lever angle. The MVCS tracked the reference point schedules well. FTIT and four burner pressure limits were accommodated where required for safe operation. The integral trims held the RCVV's and CIVV's to their respective schedules. The fan rotor speed and fan discharge $\Delta p/p$ were held to their schedules values through the use of integral trims on exhaust nozzle area and main burner fuel flow.

In general, steady-state performance of the F100 MVCS control was good at all points tested. The integral control action held scheduled variables close to their scheduled

values. Minor reference point schedule adjustments allowed schedule matching without controls saturating or engine variables exceeding allowable limits.

Transient performance was assessed at all the flight points. Large PLA transients were run at all points where air flow constraints permitted PLA operation below 83°. Small PLA transients of 3° were run to check the regulator performance while random PLA sequences were run to verify correct gain scheduling operation. In all cases, PLA was changed at a rate of $\pm$ 126°/sec. A programmable function generator was used to control the PLA during the transient tests to insure repeatability.

Good transient performance was demonstrated at almost all flight points. The integral trims successfully accommodated FTIT limits and low burner pressure limits where required. The control attenuated afterburner pressure pulses occurring during afterburner lights at all but two flight points. At supersonic points, where operation was permitted only at intermediate and above, excellent suppression of afterburner disturbances was observed. The multivariable control successfully operated the engine for random PLA excursions, thereby verifying the correct functioning of regulator gain schedules and transition logic. A number of flight maneuvers were performed to check the control's performance with simultaneously varying PLA and ambient conditions. The control tracked reference point schedules well and accommodated all limits.

Programming flexibility which exists due to the modular structure of the multivariable control was demonstrated by testing two alternate control modes. A fast acceleration set of transition control rates was implemented which allowed more rapid engine accelerations. Also, the integral trim structure was changed to use engine pressure ratio instead of the fan discharge Mach number parameter normally used

with the multivariable control. The new trim structure worked satisfactorily, requiring only a change of gain matrices to implement it.

Sensor and actuator failure detection logic was incorporated into the control for altitude tests and functioned well in conjunction with a backup control. All logic was programmed in 9500 words of core memory, using a 12 msec. computer cycle time. These computer requirements are within the capabilities of present generation computers envisioned for use as engine mounted digital controls.

Several aspects of the control implementation were studied in detail during this phase of the program. These topics, presented in the subsequent sections, include a) validation of the MVCS reference and trim schedules, b) transient performance evaluation and, c) accommodation of A/B operation.

3.2 VALIDATION OF REFERENCE POINT AND TRIM SCHEDULES

3.2.1 Reference Schedule Correlation

One goal of the extensive baseline runs of the BOM control prior to the MVCS demonstration was the validation of the data used to model the real engine operating characteristics. The test article represented a experimental demonstrator build. The instrumentation was installed for research purposes. The correlation between the observed engine operation and the nonlinear simulation of a production engine configuration was an important area of concern during the development effort.

The steady state data for the reference point schedules (excluding $\Delta p/p$) was accumulated and the match of reference values between schedules and measurements was calculated. This data is shown in Appendix B.

The agreement in most operating point variables was within an acceptable tolerance except that it was found that the engine was operating at lower fan speeds than predicted from the deck. As a result of these observations, and in order to make the multivariable control performance match the BOM operation for comparison purposes, the following changes were implemented in the control design:

(1) A constant bias was added to the scheduled corrected fan speed, i.e.

$$\left(\frac{N_1}{\sqrt{\theta_2}}\right)_{SCH,NEW} = \left(\frac{N_1}{\sqrt{\theta_2}}\right)_{SCH,OLD} - 355 \text{ RPM}$$

(2) A constant bias was added to the scheduled burner pressure ratio, i.e.

$$\left(\frac{P_B}{P_{T2}}\right)_{SCH,NEW} = \left(\frac{P_B}{P_{T2}}\right)_{SCH,OLD} - 1.54$$

3.2.2 Δp/p Instrumentation Evaluation

One important feature of the MVCS design is functional modularity. An example of this is the decoupled integral trim structure. Using this design method, the variables chosen as the engine reference points could be altered without a complete recalculation of the controller gains. The only changes to the controller involve recalculation of the integral network gains using the pole placement method described in Ref. [2].

Two trim systems were available during the altitude test. The normal trim mode ($N_1/\Delta p/p$) used fan speed and fan exit dynamic head ($\Delta p/p$) to set the fan match point with the geometry on schedule. The alternate mode selected (N_1/EPR) used fan speed and engine pressure ratio (P_{T6}/P_{T2}) to set the operating point. Integral gains had been calculated and evaluated for these modes on the hybrid simulation.

The advantages of using $\Delta p/p$ as controlled variable are illustrated in Figure 3.3 from the altitude test demonstration. In this experiment, fan speed was manually held constant which nozzle area was changed. It is evident that $\Delta p/p$ is near independent of fan speed while EPR response is strongly coupled to both speed and area (see Ref. 2). Thus, $\Delta p/p$ is more attractive to set performance with fan speed because of the nearly orthogonal static relationship (see Figure 3.4). This static relationship is also valid during the integral trim dynamic action since in the trim time frame, all engine responses are essentially quasi-static. The major disadvantage to $\Delta p/p$ for the MVCS demonstration was the lack of a well documented instrument correlations available since this parameter was not used within the BOM control.

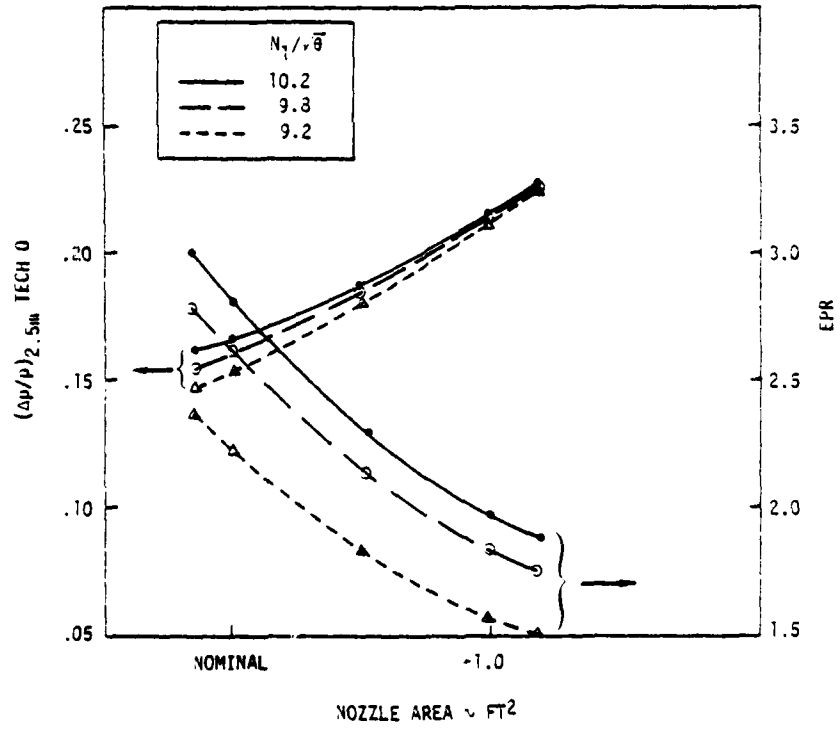

Figure 3.3 Area Variation at Constant Speed

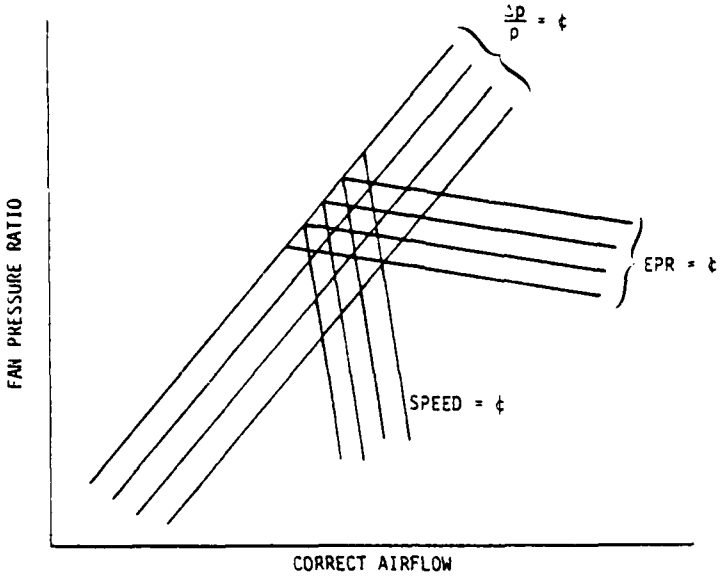

Figure 3.4 Relationship of ΔP/P to EPR on Fan Map

Development and experimental evaluation of suitable instrumentation for Δp/p was required for this mode. Three alternative data sampling and data processing techniques for investigating fan exit Mach number of $(\Delta p/p)_{2.5m}$ characteristics at all flight conditions during the BOM testing are specified in Appendix C. The purpose of specifying these alternatives was to determine the minimum complement of total and static pressure transducers necessary to synthesize accurately fan exit Δp/p for the MVCS evaluation. The data obtained for this study was limited to subsonic conditions at simulated altitudes of 10,000 feet, 30,000 feet and 45,000 feet. The following results, conclusions and discussion apply, therefore, to subsonic MVCS testing only. BOM testing at supersonic conditions followed by a less complete Δp/p analysis preceded the MVCS testing utilizing $(\Delta p/p)_{2.5m}$ to control the fan match point.

The important questions that were addressed by this study include the following:

(1) What were the XD11 fan exit $(\Delta p/p)_{2.5m}$ characteristics at the flight conditions tested compared to the original MVCS schedule?

(2) What is the effect of a $(\Delta p/p)_{2.5m}$ error on the fan match?

(3) What reduced set of measurements for total and static pressures should be used for the MVCS testing?

(4) How can the reduced set of measurements be utilized to synthesize the correct average fan exit $(\Delta p/p)_{2.5m}$?

(5) What techniques should be used to insure continuous engine operation at other flight conditions or in case of a critical sensor failure?

The following summary of results is presented as a reference to the major sections of Appendix C and to provide an overview of the quantitative findings:

(1) The XD11 fan exit $(\Delta p/p)_{2.5m}$ characteristics were similar to the current MVCS schedule at all flight conditions but contained a +0.045 bias at all airflows.

(2) The maximum effect of a 10% error in $(\Delta p/p)_{2.5m}$ was a 5% change in fan pressure ratio at constant corrected airflow.

(3) The locations which may be used to measure total and static pressures are shown in Table 3.2.

(4) In order to synthesize the correct average fan exit $(\Delta p/p)_{2.5m}$ using the sensors defined in (3), set CC3 = 0.46445, CF3 = 0.56825, and CD3 = 0.0 in the current calculation of $(\Delta p/p)_{2.5m}$ (see Table 3.3).

(5) In order to ensure continuous engine operation at flight conditions not previously tested during the BOM tests $(\Delta p/p)_{2.5m}$ deviation limits of $\pm 25\%$ of schedules may be checked. If these limits are exceeded, then the calculation of $(\Delta p/p)_{2.5m}$ should be performed using the full complement of validation station 2.5 total and static pressures (technique 0).

Table 3.2

Station Location for $\Delta p/p$ Synthesis

	CORE (HOT) SIDE - 2.5_H		FAN (COLD) SIDE - 2.5_F	
	CIRCUM. LOC.	PROBE #	CIRCUM. LOC.	PROBE #
TOTAL PRESSURE	113°	2	248°	2
STATIC PRESSURE	278°	O.D.	264°	O.D.

Table 3.3

F100 (XD11) Fan Exit $\Delta p/p$ Instrumentation Recommendation

$$\Delta p/p_{2.5\text{measured}} = 0.46445 \quad \frac{\bar{P}_{T2.5C3} - \bar{P}_{S2.5C3}}{\bar{P}_{T2.5C3}} + 0.56825x$$

$$\frac{\bar{P}_{T2.5F3} - \bar{P}_{S2.5F3}}{\bar{P}_{T2.5F3}} + 0.045$$

where the probes used are:

$\bar{P}_{T2.5C3}$: core side at 113°, probe number 2
$\bar{P}_{T2.5F3}$: fan side at 248°, probe number 2
$\bar{P}_{T2.5C3}$: core side at 278°, O.D. probe
$\bar{P}_{S2.5F3}$: fan side at 264°, O.D. probe

The following qualitative conclusions were reached as a result of BOM testing:

- The F100 (XD11) measured $(\Delta p/p)_{2.5m}$ was within acceptable tolerances as determined during the MVCS design using F100 simulation data.
- A small bias shift in the current schedule could be implemented by shifting the T2 bias, or the base $(\Delta p/p)_{2.5m}$ schedule. The new $(\Delta p/p)_{2.5m}$ schedule will then match the measured $(\Delta p/p)_{2.5m}$ within acceptable tolerances.
- The MVCS tests could have been normally executed using the minimum set of total and static pressure measurements specified in the results. However, backup calculations of $(\Delta p/p)_{2.5m}$ using all available and valid station 2.5 pressure measurements were retained during test.

Based upon the instrument recommendations, the altitude test demonstration was undertaken with the technique 0 synthesis method. Additional data was acquired using the specified channel combinations which further validate the results presented in Appendix C.

3.3 TRANSIENT CONTROLLER PERFORMANCE

Transient power and flight point maneuvers were performed during the demonstration. A complete discussion of these results is contained in Ref. 2. Several phenomena were observed during the testing which required minor modification of the control software. These effects are discussed in detail below.

3.3.1 General Response Characteristics

The dynamic response of the control was nearly identical to that observed during the hybrid evaluation. Figure 3.5 shows a comparison of the MVCS and BOM behavior during a throttle bodie (i.e., chop-hold-snap). Augmentor pressure (P_{T6}) is shown as a relative thrust response parameter. A small hysteresis is evident in both control responses due primarily to actuator uncertainties. The multivariable control responses are symetric during the maneuver primarily because of the linear feedback control form. The production control uses nonlinear logic to operate the nozzle area during transient maneuvers. The integral trim time constants are clearly visible in both controllers. No modifications were made to the control gains, transition model or integrator logic during the test program. Both normal and fast response transition models were tested. This aspect of the test results alone is an important result regarding the effectiveness and applicability of the MVC design procedure in conjunction with the hybrid evaluation approach.

3.3.2 Fuel Valve Anomalies

An anomaly in the electromechanical servovalve used to meter fuel flow to the engine was noted during the demonstration. This phenomena occurred only at low fuel flows as illustrated in Figure 3.6. Fuel spikes were noted in the fuel servo feedback and flowmeter outputs in response to constant fuel commands. Operation of the control logic was altered to limit fuel command excursion during decels above this critical flow region. This accommodation capability was already available in the integral trim logic which prevents integrator windup during operation with saturated actuator channels [2].

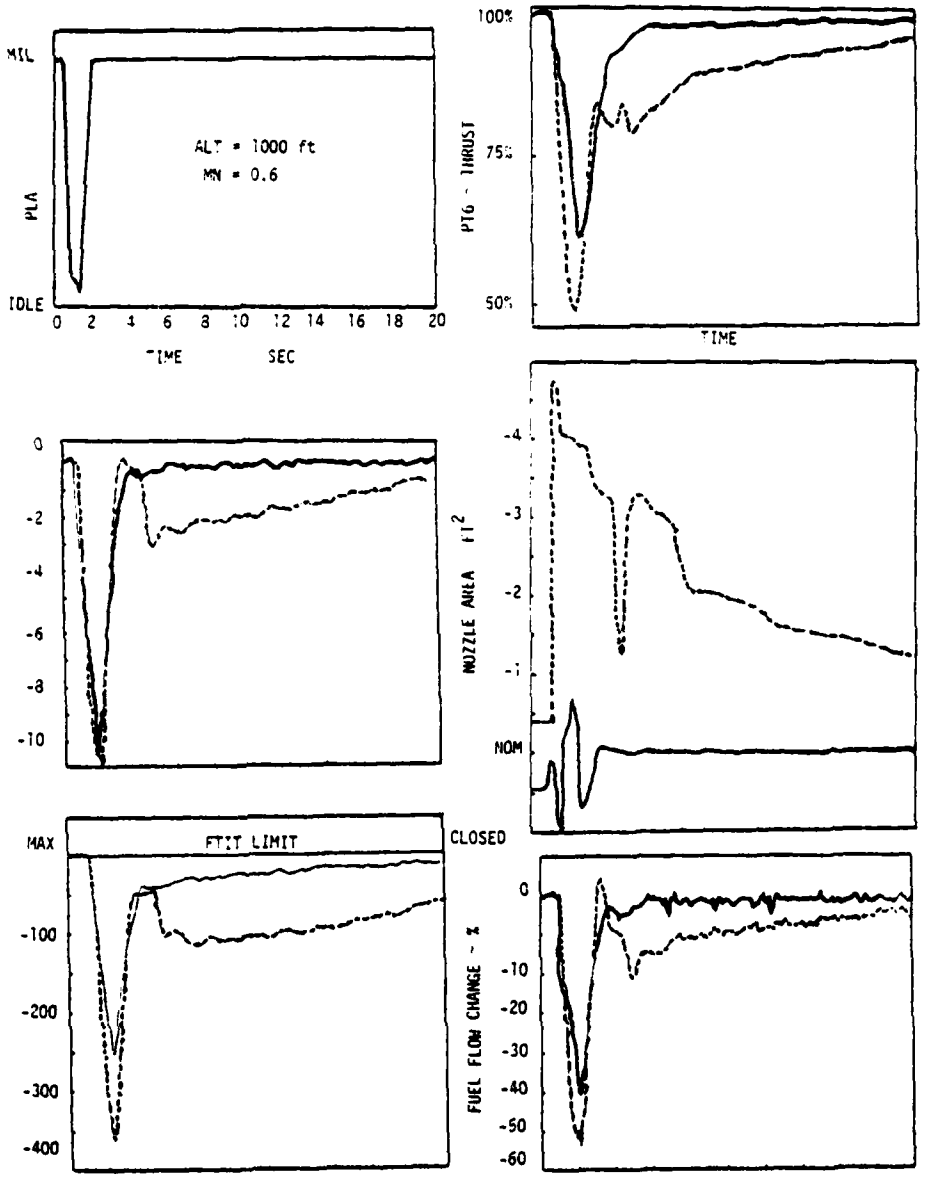

Figure 3.5 Comparison of MVC and BOM Bodie Response

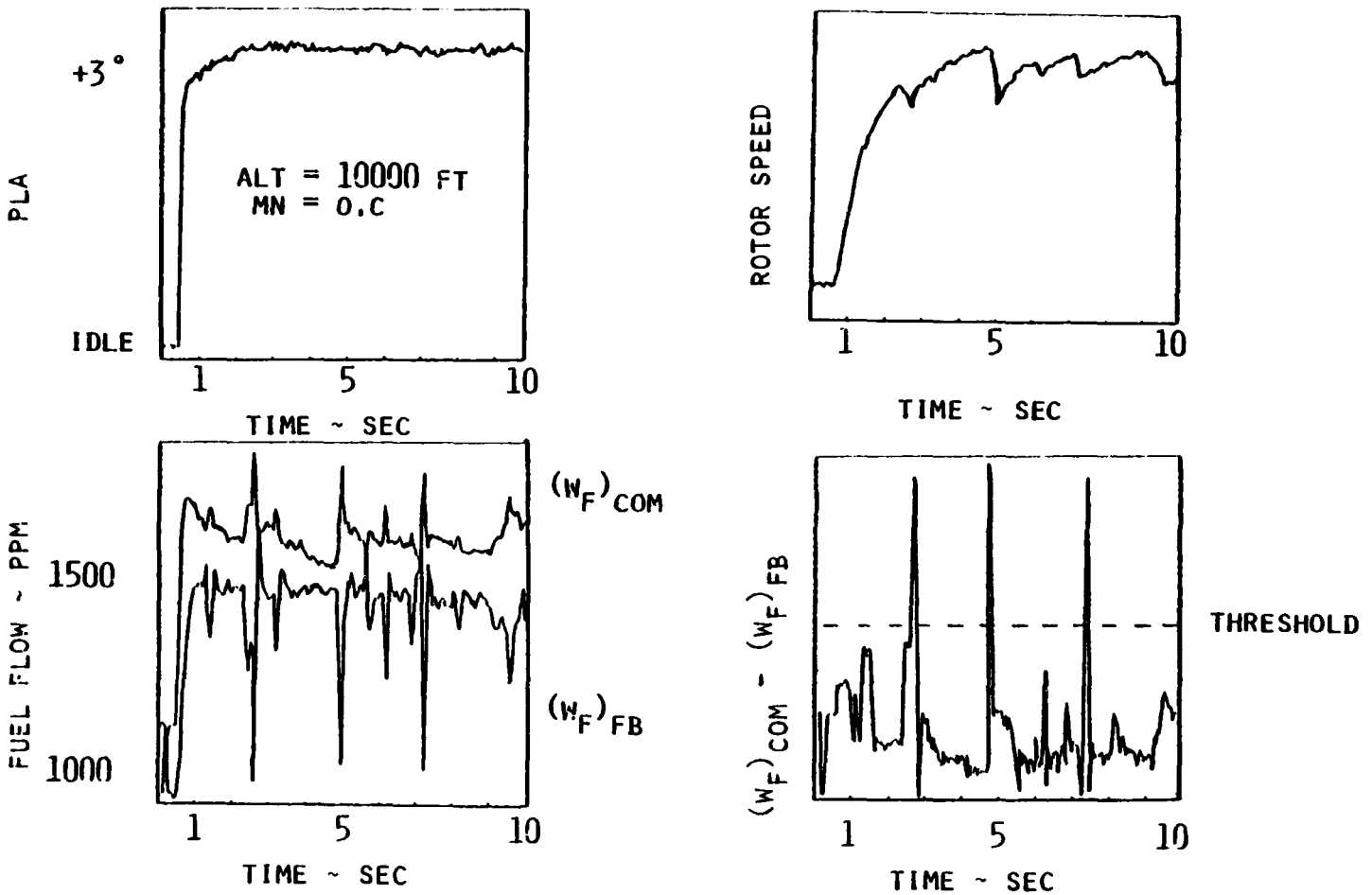

Figure 3.6 Erratic Fuel Valve Behavior

3.3.3 Test Facility Interaction

During large engine transients, the variation of engine airflow caused significant air supply transients in the PSL facility. These effects were more pronounced during operation at lower pressures and physical airflows. They appeared in both BOM and MVCS operation. During MVCS operation, the variation in engine face pressure (i.e. a pressure decrease caused by an increase in engine airflow and speed) coupled through the reference schedules to provide a destabilizing dynamic effect.

This phenomenon is shown in Figure 3.7. An initial fan speed drop (due to an A/B light) causes engine face pressure increases. The air supply facility sees an equivalent drop in airflow through the engine. Engine pressure (P_{T2}) increases, which causes the reference schedules to increase the fuel flow and P_{T6} reference values. The scheduled fan speed drops because of a temperature increase. As the engine speed responds to these schedule variations, the time lag in the facility air supply, engine response and integral time constants couple to produce the underdamped behavior illustrated in the figure.

This dynamic interaction is peculiar to the facility dynamics involved. This response was not observed during pressure variation testing on the digital or hybrid simulation. At flight conditions where large physical airflows were available, the change in airflow for a change in engine speed was a much smaller percentage of total airflow and the dynamic interactions were not observed.

3.3.4 Turbine Temperature Limiting

To compensate for the fan turbine inlet temperature (FTIT) thermocouple response time constant, the MVCS included a two input estimator for FTIT which use a pole placement

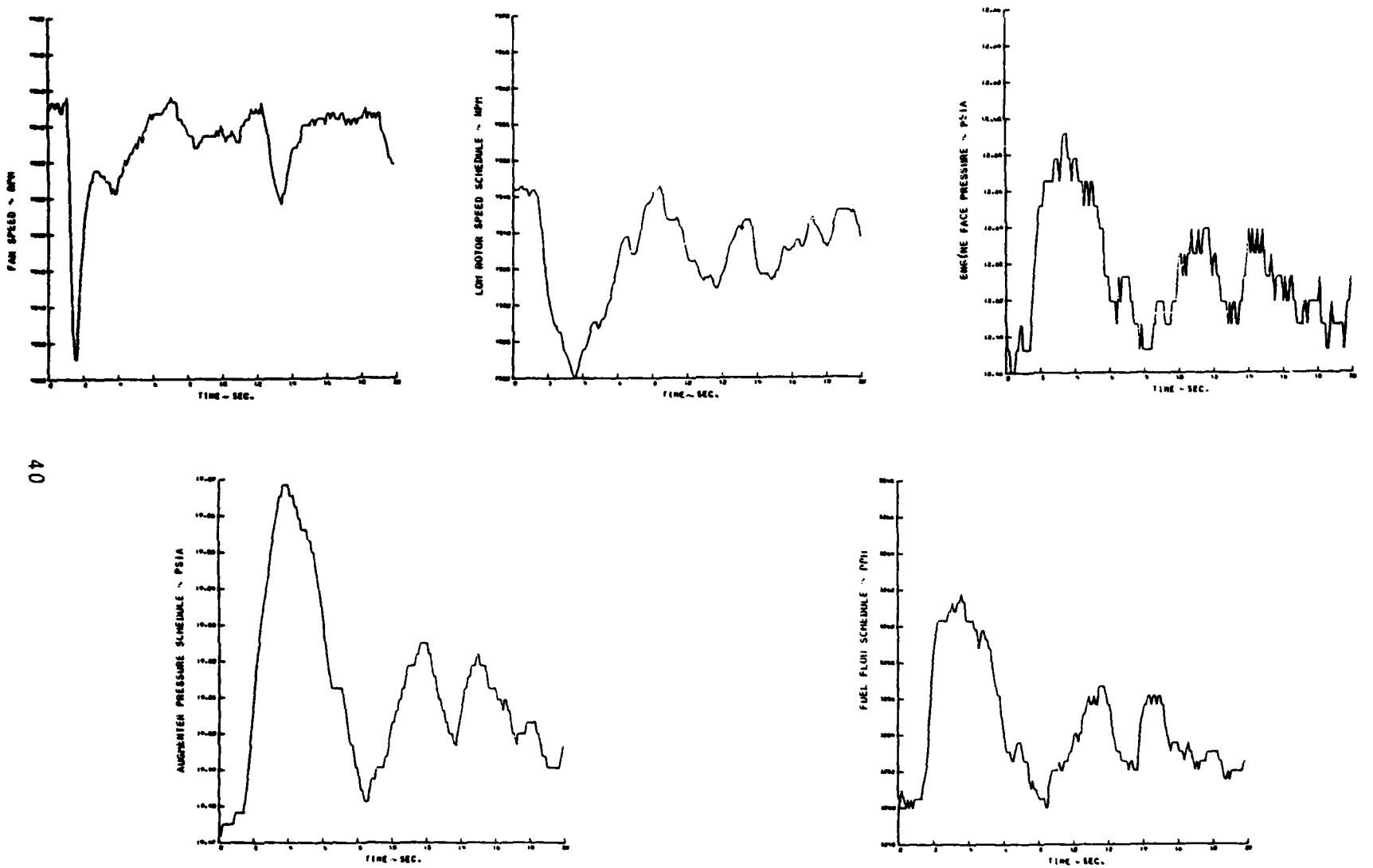

Figure 3.7 Facility Air Supply/Engine Interaction During Test of MVC Logic

structure to provide shaped frequency response to fuel flow and the FTIT probe signal. A reference schedule input is used as a feedforward. The estimator output is only active at intermediate power when the temperature limit is active. For the test implementation the maximum turbine temperature limit was lowered 20°F. In addition, the engine characteristics indicated that the nominal fuel-to-temperature curves were not accurate for the XD11. These two effects cause the MVCS to temperature limit significantly below intermediate throttle level. In order to accommodate this effect, the feedforward schedules in the estimator were altered to represent the modified fuel/temperature curves observed for the XD11. Excellent response was then obtained as shown in Figure 3.8. Since this may be representative of the worst case variation observed in installed engines, these tests indicate that a more sophisticated filtering approach would be appropriate for estimation of turbine temperature. Since filtering and estimation concepts were specifically not addressed during the MVCS development, this area would merit further study.

A group of implementation details observed during the PSL demonstration have been described. These conditions were alleviated with minor logic modification and, in general, the MVCS design performed during the PSL demonstration without modification to the function and structure.

3.4 AFTER BURNER ACCOMMODATION

At several of the tested altitude conditions, power transients were prohibited because of inlet airflow schedules and minimum burner pressure requirements. In order to exercise the logic, a disturbance input was made to the engine in the form of an afterburner ignition. The MVCS does not include A/B accommodation logic; thus, this input

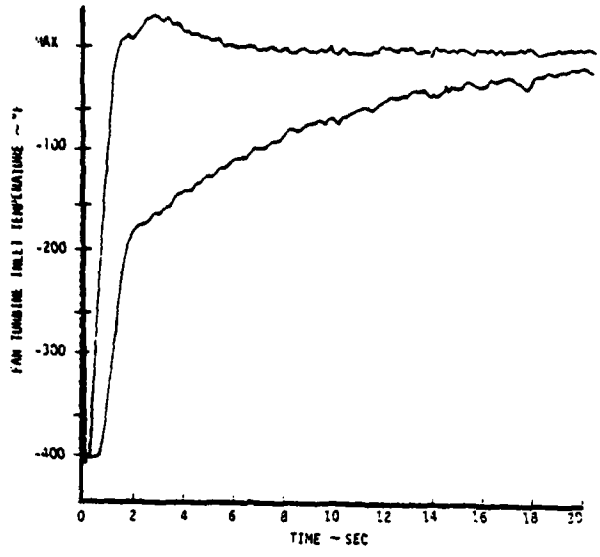

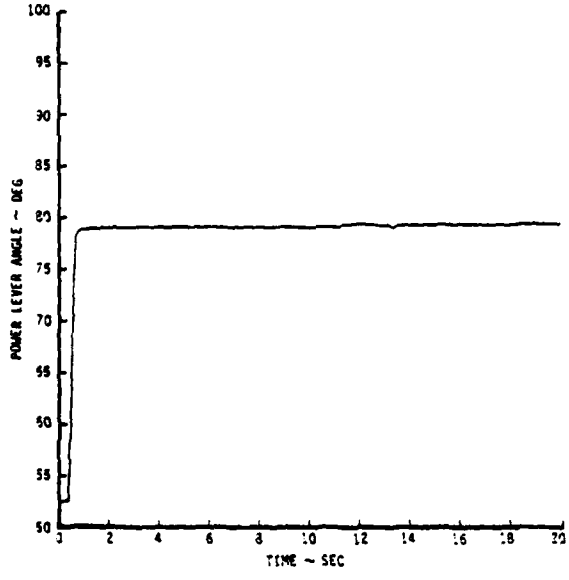

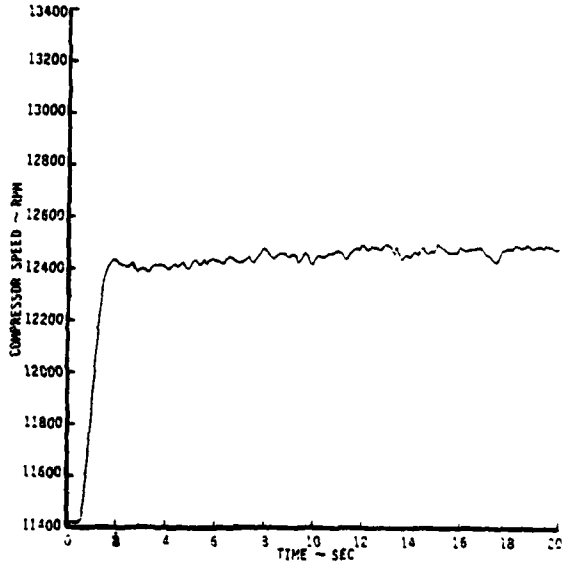

Figure 3.8 Performance of Updated FTIT Estimator During Shap Acceleration to Temperature Limited Condition (MVC Engine Test -- Alt=10K, Mn=0.6)

causes the MVCS to accommodate virtually a step disturbance input.

Augmentor fuel was metered at the initial ignition flow to the innermost (segment I) flameholder (see Figure 3.9). The ignition pulse produced a back pressure which causes engine speed to drop and turbine inlet temperature to rise. The nozzle must be opened to accommodate the additional tailpipe pressure. Over the flight envelope, the MVCS performed comparably to the hybrid evaluation results in attenuating A/B

Figure 3.9 Afterburner of F100 Engine

ignition pulses measured by the size of the observed P_{T6} pulse. In Figure 3.10, the performance of the MVCS and the BOM are compared against the control design specification determined at the beginning of the program [3].

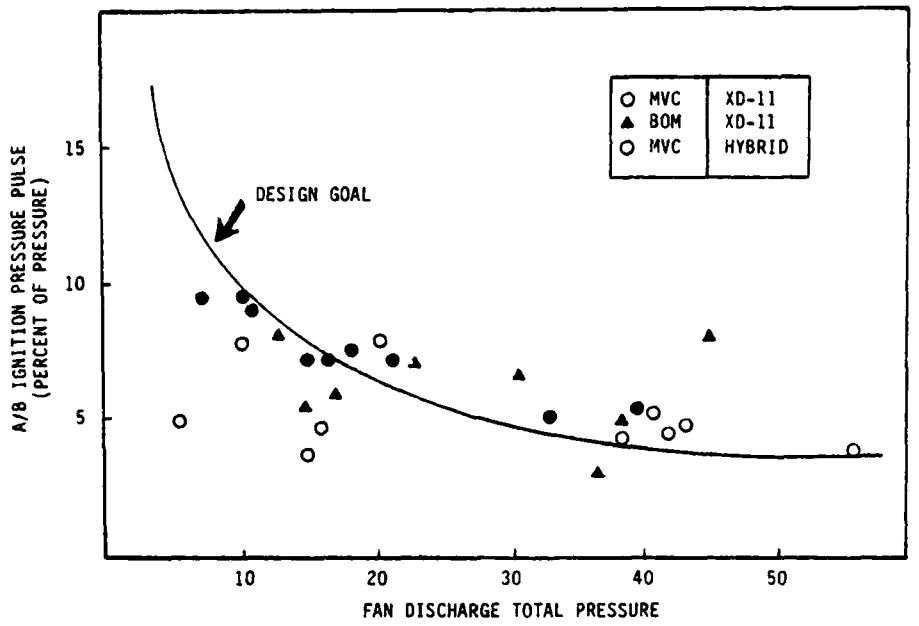

Figure 3.10 Afterburner Suppression Curve

3.5 SUMMARY

A short summary of the F100/MVCS altitude cell demonstration has been presented. Several topics have been examined as they affected the response of the system during test. The validation of the steady state reference and trim schedules is described. Transient performance is summarized and several logic changes delineated. The performance of the control during A/B transients is described and afterburner suppression relative to the design goals is established.

CHAPTER IV

SUMMARY AND PERSPECTIVE

4.1 SUMMARY

Modern aircraft turbine engines include a variety of control actuators which affect the performance and response of the propulsion plant. The incorporation of digital processing permits integrated control action to meet strict steady-state and transient performance requirements. The need exists for a control design procedure that can account for multiple loop interaction and can make efficient use of them to enhance performance without decreasing engine stability margins. The F100 Multivariable Control Synthesis Program was a cooperative effort with the Aero Propulsion Laboratory and the NASA Lewis Research Center aimed at investigating the use of extended linear quadratic synthesis techniques to accomplish the design, evaluation and testing of a practical multivariable control for the F100 engine.

A digital, multivariable control design procedure for the F100 turbofan engine is described. The controller is based on locally linear synthesis techniques using linear, quadratic regulator design methods. The control structure uses an explicit model reference form with proportional and integral feedback near a nominal trajectory. Modeling issues, design procedures for the control law and the estimation of poorly measured variables are presented.

The multivariable control law was implemented on a general purpose minicomputer at NASA Lewis Research Center. The logic was thoroughly validated against explicit design and operating performance criteria on a real time hybrid simulation of the engine throughout the full flight envelope.

Alternate control modes, sensor failure sensitivities and other design features were investigated using the hybrid simulation.

The resulting system was then used to operate an actual F100 engine in an altitude test facility at NASA Lewis Research Center. In all, steady-state and transient performance were investigated at five subsonic and four supersonic test points. The results of these experiments and correlation to the important design issues are presented.

4.2 A LOOK AT THE FUTURE

The micro-electronic revolution has already significantly affected turbine engine controls. This capability alone would not radically alter the hydromechanical hardware on current commercial and military turbines because these systems have a long reputation for reliability and cost effectiveness. However, near-term propulsion system requirements for V/STOL and military flight applications cannot be realized with purely hydromechanical devices. The performance capability of these propulsion systems is now dependent on the control rather than the components. Practical designs integrating engine, inlet, and airframes will be necessary. Multivariable procedures must be used to accommodate dynamic and static interactions which will dominate these system configurations. Proposed V/STOL applications, for example, have propulsion system components, gas generators, fans, ducts, mechanical linkages, etc. distributed throughout the airframe. A design method to make this type of system operable is imperative.

Linear quadratic techniques are one solution. Frequency domain design has been developing swiftly to realize classical stability criteria designs with which many people are more familiar. Multivariable stability and direct stability

margin design for time domain systems is coming. All of these techniques, for turbine engines, must be blended with the static performance and large transition requirements which often predominate the control design. New requirements for reliability seem to dictate highly robust systems or, more likely, specifically fault accommodating. Total integration of the propulsion system with the airframe demands a decentralized design with data and command links from several control processing locations in the vehicle. Obviously, regulator synthesis is only a small part of the global propulsion design.

Recent work in advance techniques has shown promise. Merril [5] at NASA Lewis had performed direct output regulator designs for the F100 models. Comparison between LQR results have shown essentially the same behavior. Output regulator design allows a greater flexibility for direct fixed structure optimization and multiplant design unavailable in LQR procedure. The importance of this procedure is that high order linear models do not penalize the control law with redundant and difficult to estimate feedback terms. Indeed, the procedure can be used to validate designs produced by LQR synthesis.

Teren [6] has presented work in optimal trajectory generation using a cost function linear in the states and controls with constraints on the outputs. The procedure can improve nominal path algorithms for large transitions. Several authors have addressed sensor failure accommodating filters and control architectures.

The evolution of multivariable, electronic controls for complex turbine propulsion systems is in full swing. Next generation engines will have the hardware and the requirement. Optimal control procedures and locally linear design techniques offer a strong option to design engineers for the development of the high performance, high reliability, cost-effective systems which are needed.

REFERENCES

1. Szuch, J.R., Soeder, J.F., Seldner, K., and Cwynar, D.S., "F100 Multivariable Control Using a Real-Time Engine Simulation," NASA TP-1056, 1977.

2. De Hoff, R.L., Hall, W.E., Jr., Adams, R.J., and Gupta, N.K., "F100 Multivariable Control Synthesis Program – Vol. I: Development of F100 Control System," Systems Control, Inc. (Vt), Palo Alto, CA, Final Report, 1 August – 31 December 1976, June 1977 (AFAPL-TR-77-35-Vol. 1, AD-A-52420).

3. Miller, R.J. and Hackney, R.D., "F100 Multivariable Control System Engine Models/Design Criteria," Pratt & Whitney Aircraft, West Palm Beach, FL, PWA-FR-7809, August 1976 (AFAPL-TR-76-74).

4. Szuch, J.R., Skira, C., and Soeder, J.F., "Evaluation of an F100 Multivariable Control Using a Real-Time Engine Simulation," NASA TM X-73648, 1977.

5. Merrill, W.C., "Design of Turbofan Engine Controls Using Output Feedback Regulator Theory," presented at the 1977 JACC, San Francisco, CA, June 1977.

6. Teren, F., "Minimum Time Acceleration of Aircraft Turbine Engines," NASA TM X-73624, June 1977.

APPENDIX A

F100 MULTIVARIABLE CONTROL DESIGN RELATED LITERATURE

1. Adams, R.J., De Hoff, R.L., and Hall, W.E., Jr., "Modeling and Instrumentation Requirements for Multivariable Control of an Advanced Turbofan Engine," AIAA Paper 77-834, July 1977.

2. Cwynar, D.S., "INFORM: An Interactive Data Collection and Display Program with Debug Capability," NASA TP-1424, 1979.

3. De Hoff, R.L., "Multivariable Control Design Principles with Application to F100 Turbofan Engine," JACC 1976, Paper APPL 2/2.

4. De Hoff, R.L. and Hall, W.E., Jr., "Design of a Multivariable Controller for an Advanced Turbofan Engine," Conference on Decision and Control and Symposium on Adaptive Processes, 15th, Institute of Electrical and Electronic Engineers, Inc., 1976, pp.1002-1008.

5. De Hoff, R.L. and Hall, W.E., Jr., "Jet Engine Systems Modeling: State Space Techniques and Modeling for Control," Advances in Control and Dynamic Systems, Vol. XIV, C.T. Leondes, Editor, Academic Press, New York, N.Y., 1977.

6. De Hoff, R.L. and Hall, W.E., Jr., "Multivariable Control Design Principles with Application to the F100 Turbofan Engine," Productivity: Proceedings of the Joint Automatic Control Conference, American Society of Mechanical Engineers, New York, 1976, pp.113-116.

7. De Hoff, R.L., Hall, W.E., Jr., Adams, R.J., and Gupta, N.K., "F100 Multivariable Control Synthesis Program — Vol. I: Development of F100 Control System," Systems Control, Inc. (Vt), Palo Alto, CA, Final Report, 1 August — 31 December 1976, June 1977 (AFAPL-TR-77-35-Vol. 1, AD-A-52420).

8. De Hoff, R.L. and Hall, W.E., Jr., "System Identification Principles Applied to Multivariable Control Synthesis of the F100 Turbofan Engine," presented at the 1977 JACC, San Francisco, CA, June 1977.

9. De Hoff, R.L. and Hall, W.E., Jr., "Multivariable Quadratic Synthesis of an Advanced Turbofan Engine Controller," Journal of Guidance and Control, Vol. 1, No. 2, March–April 1978, pp.136-142.

10. Lehtinen, B., Soeder, J.F., Costakis, W., and Seldner, K., "Altitude Tests of a Multivariable Control for the F100 Turbofan Engine," Proposed NASA Technical Paper.

11. Lehtinen, B., De Hoff, R.L. and Hackney, R.D., "Multivariable Control Altitude Demonstration on the F100 Turbofan Engine," AIAA 79-1204, 15th SAE-AIAA Propulsion Conference, Las Vegas, Nevada, 1979.

12. Miller, R.J. and Hackney, R.D., "F100 Multivariable Control System Engine Models/Design Criteria," Pratt & Whitney Aircraft, West Palm Beach, FL, PWA-FR-7809, August 1976 (AFAPL-TR-76-74).

13. Merrill, W.C., "Design of Turbofan Engine Controls Using Output Feedback Regulator Theory," presented at the 1977 JACC, San Francisco, CA, June 1977.

14. Soeder, J.F. and Cwynar, D.S., "Real-Time Computer Implementation of a Multivariable Control for the F100 Turbofan Engine," Proposed NASA Technical Paper.

15. Szuch, J.R., Seldner, K., and Cwynar, D.S., "Development and Verification of a Real-Time, Hybrid Computer Simulation of the F100-PW-100(3) Turbofan Engine," NASA TP-1034, September 1977.

16. Szuch, J.R., Skira, C., and Soeder, J.F., "Evaluation of an F100 Multivariable Control Using a Real-Time Engine Simulation," NASA TM X-73648, 1977.

17. Szuch, J.R., Soeder, J.F., Seldner, K., and Cwynar, D.S., "F100 Multivariable Control Using a Real-Time Engine Simulation," NASA TP-1056, 1977.

18. Teren, F., "Minimum Time Acceleration of Aircraft Turbine Engines," NASA TM X-73624, June 1977.

19. Weinberg, Marc S., "A Multivariable Control for the F100 Engine Operating at Sea-Level Static," ASD-TR-75-28, November 1975.

20. Zeller, J.R., Arpasi, D.J., and Lehtinen, B., "A Digital Computer Propulsion Control Facility – Description of Capabilities and Summary of Experimental Program Results," presented at NASA ACT Conference, 11 July 1974.

APPENDIX B
REFERENCE POINT SCHEDULE EVALUATION

The analysis of BOM data to validate the reference point schedules is documented below. This data includes steady state and transient operation of the engine at flight points, K, F, C, E, and L between intermediate and idle power. The objective of the analysis was to evaluate the operation of the MVC following the BOM controller and to recommend adjustments to the digital schedules to account for peculiarities in the PSL instrumentation or the engine.

CONCLUSIONS AND RECOMMENDATIONS

The agreement between schedules and actual values of NH, FTIT, $\frac{PT6}{PT2}$ and $W_{f_{corrected}}$ are acceptable. The $NL_{corrected}$ and $\frac{PB}{PT2}$ schedules were, however, modified. Specifically, the $NL_{corrected}$ schedule should have a constant bias of 355 RPM subtracted, and the $\frac{PB}{PT2}$ schedule should have a constant bias of 1.54 subtracted.

DATA

Figures 1 through 6 are plots of F100 (XD11) operating line data. Each operating line is indicated in the figures by a different symbol. Specifically

- ◖: 45,000 ft, M-0.9
- ■: 30,000 ft, M=0.9
- ▲: 10,000 ft, M=0.6
- ●: 10,000 ft, M=0.9
- ◤: 10,000 ft, M=1.2

The test data have been plotted against their scheduled values. Consequently, a perfect match corresponds to data points falling on the "45 degree" line. The figures are

Figure 1: $(NL)_{\substack{actual \\ corrected}}$ vs. $(NL)_{\substack{scheduled \\ corrected}}$

Figure 2: $(NH)_{actual}$ vs. $(NH)_{scheduled}$

Figure 3: $(FTIT)_{actual}$ vs. $(FTIT)_{scheduled}$

Figure 4: $(\frac{PT6}{PT2})$ vs. $(\frac{PT6}{PT2})_{scheduled}$

Figure 5: $(\frac{PB}{PT2})_{actual}$ vs. $(\frac{PB}{PT2})_{scheduled}$

Figure 6: $(W_f)_{\substack{actual \\ corrected}}$ vs. $(W_f)_{\substack{scheduled \\ corrected}}$

The revised schedules are included in Figures 1 and 5. The bias levels indicated were found by averaging the errors between the actual data and the scheduled values.

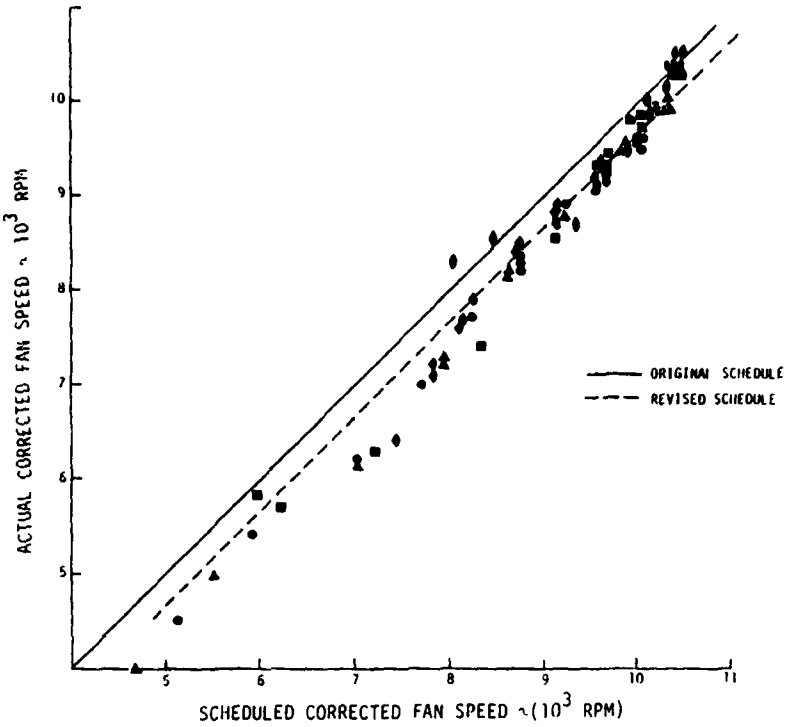

Figure 1 Comparison of Actual and Scheduled Corrected Fan Speed at Subsonic Test Points

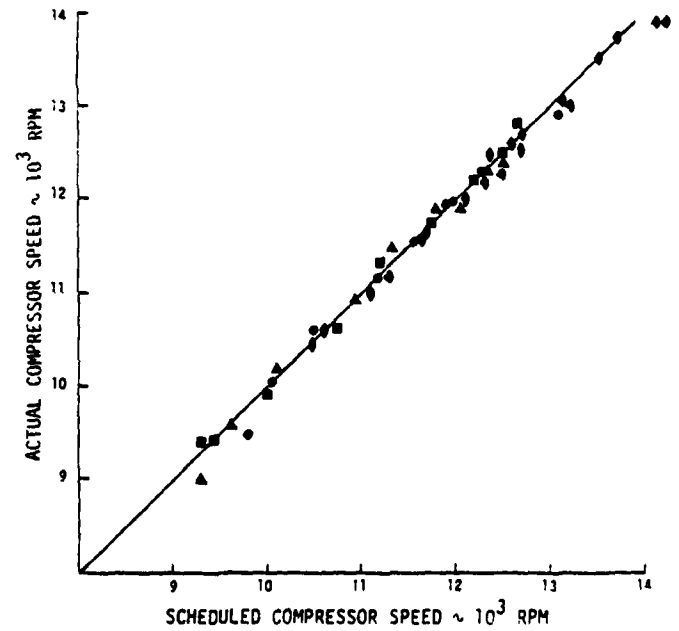

Figure 2 Comparison of Actual and Corrected Compression Speed at Subsonic Test Points

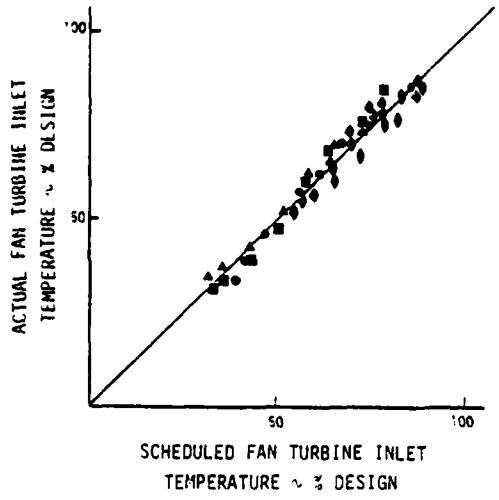

Figure 3 Comparison of Actual and Scheduled Fan Turbine Inlet Temperature at Subsonic Test Points

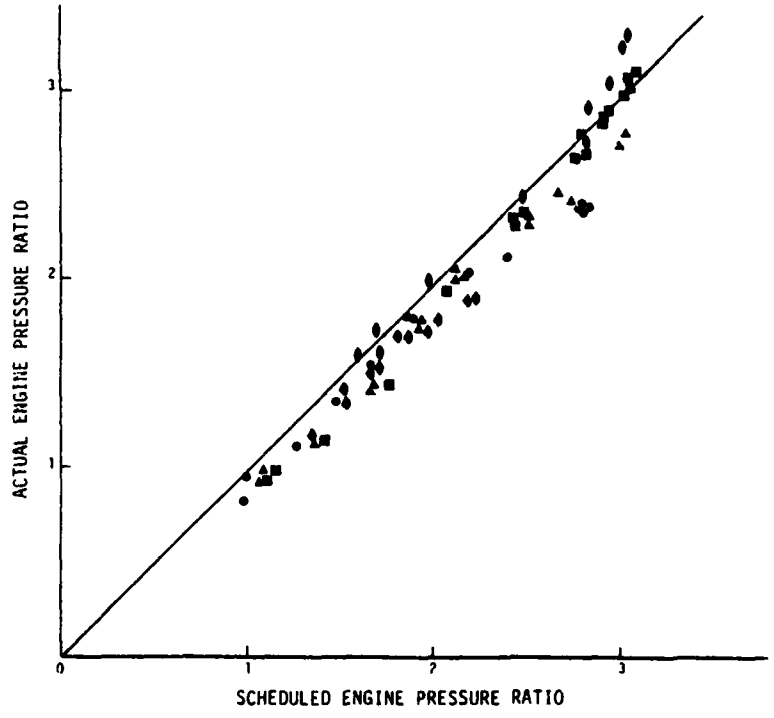

Figure 4 Comparison of Actual and Scheduled Engine Pressure Ratio at Subsonic Test Points

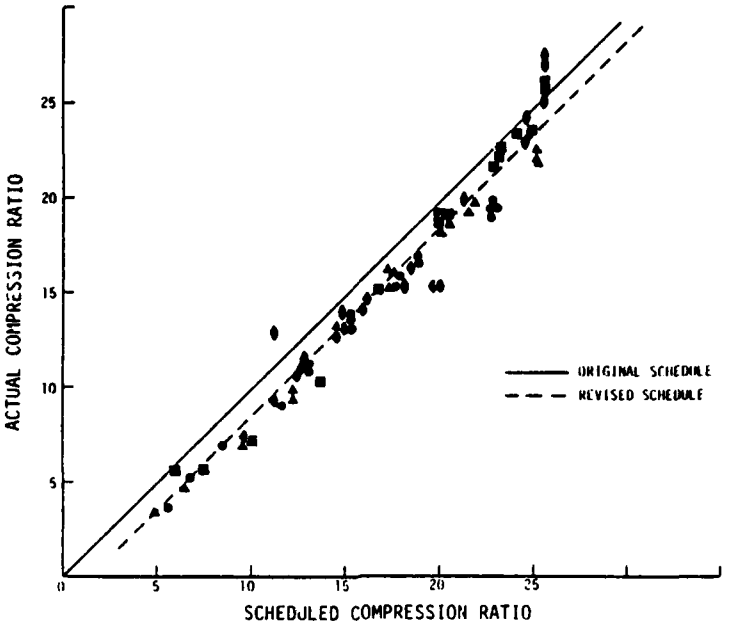

Figure 5 Comparison of Actual and Scheduled Compression Ratio at Subsonic Test Points

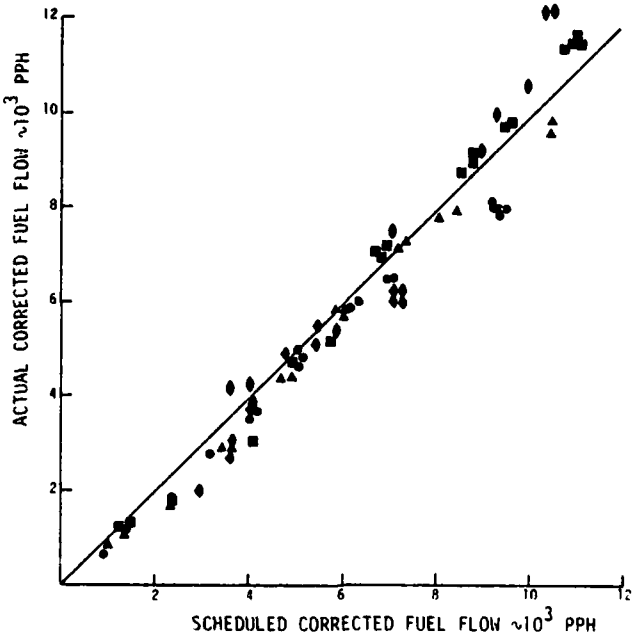

Figure 6 Comparison of Actual and Scheduled Corrected Fuel Flow at Subsonic Test Points

APPENDIX C
ANALYSIS OF ΔP/P INSTRUMENTATION

This appendix presents a detailed explanation of the data collected, the data processing techniques and the data analysis which led to the results and conclusions presented in Section III. Figure 1 illustrates the available total and static pressure transducers on XD11. The core engine or "hot" gas stream portion of the fan exit (station 2.5) had 3 point total pressure rakes at the 23°, 113° and 293° circumferential locations. Static pressure measurements in the core stream were made at the I.D. and O.D. positions at the 37°, 98°, and 278° circumferential locations. On the duct or "cold" gas stream portion of the fan exit, 3 point total pressure rakes were installed at the 68°, 248°, and 338° circumferential locations. Static pressure measurements in the duct stream were made at the I.D. and O.D. positions at the 84°, 264°, and 321° circumferential locations.

The full complement of these fan exit totals and static pressure measurements were used to calculate the best estimate of the "correct" fan exit $(\Delta P/P)_{2.5m}$. This calculation technique is presented in Table 1. As shown in Table 1, technique 0 used 9 measurements for each total pressure and 6 measurements for each static pressure. Similarly, techniques 1, 2, and 3 are presented in Tables 2, 3, and 4, respectively. Basically, each of these techniques employed less and less instrumentation to estimate fan exist $(\Delta P/P)_{2.5m}$. In the minimum instrumentation case, technique 3, only one measurement was used for each total or static pressure. The sensor complement recommended for this method is as follows:

TOTAL PRESSURE	STATIC PRESSURE
Core: 113° - 2	98° - O.D.
Fan: 248° - 2	264° - O.D.

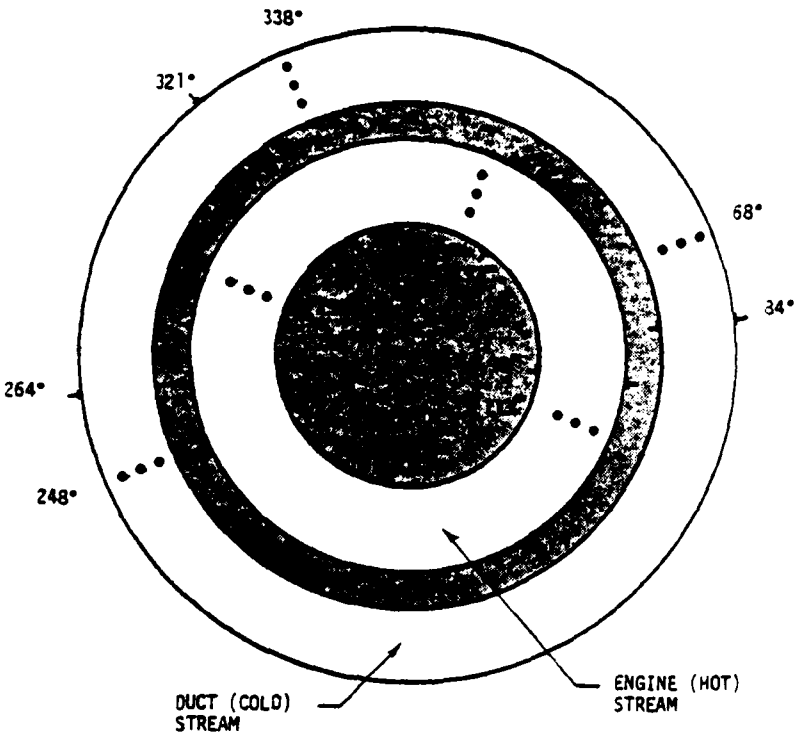

Figure 1 Fan Display Instrumentation Available on XD-11

Table 1

Technique 0 – Calculation Procedure Using Nine Total Probes and Six Static Probes for Each Intermediate Average

INTERMEDIATE AVERAGE	RANGE OF BOSS AND IMMERSION
$\overline{P}_{T2.5C0} = @(PT25 - \alpha - \beta)$	α = 23, 113, 293 β = 1, 2, 3
$\overline{P}_{T2.5F0} = @(PT25F - \alpha - \beta)$	α = 68, 248, 338 β = 1, 2, 3
$\overline{P}_{S2.5C0} = @(PS25 - \alpha - \beta)$	α = 37, 98, 278 β = I, 0
$\overline{P}_{S2.5F0} = @(PS25F - \alpha - \beta)$	α = 84, 264, 321 β = I, 0

$$(\Delta P/P)_{2.5C0} = 1 - (\overline{P}_{S2.5C0} / \overline{P}_{T2.5C0})$$

$$(\Delta P/P)_{2.5F0} = 1 - (\overline{P}_{S2.5F0} / \overline{P}_{T2.5F0})$$

} FORMULA

$$(\Delta P/P)_{2.5M0} = C_{C0} \cdot (\Delta P/P)_{2.5C0} + C_{F0} \cdot (\Delta P/P)_{2.5F0} + C_{00}$$

NOTE: @ indicates average over all bosses (α) and immersions (β) shown in range column.

Table 2

Technique 1 – Calculation Procedure Using Two Core and Fan Rakes for Intermediate Total Averages and All Static Probes

INTERMEDIATE AVERAGE	RANGE OF BOSS AND IMMERSION
$\overline{P}_{T2.5C1} = @(PT25 - \alpha - \beta)$	α = 23, 118, 014, 28, 293 β = 1, 2, 3
$\overline{P}_{T2.5F1} = @(PT25F - \alpha - \beta)$	α = 68, 248 or 68, 338 or 248, 338 β = 1, 2, 3
$\overline{P}_{S2.5C1} = @(PS25 - \alpha - \beta)$	α = 27, 98, 378 β = I, 0
$\overline{P}_{S2.5F1} = @(PS25F - \alpha - \beta)$	α = 84, 264, 321 β = I, 0

$$(\Delta P/P)_{2.5C1} = 1 - (\overline{P}_{S2.5C1} / \overline{P}_{T2.5C1})$$

$$(\Delta P/P)_{2.5F1} = 1 - (\overline{P}_{S2.5F1} / \overline{P}_{T2.5F1})$$

FORMULA

$$(\Delta P/P)_{2.5_{MI}} = C_{C1} \cdot (\Delta P/P)_{2.5C1} + C_{F1} \cdot (\Delta P/P)_{2.5F1} + C_{01}$$

VARIATION FACTORS TO TECHNIQUE 0
$\% \Delta\overline{P}_{T2.5C1} = 100 \cdot (1 - [\overline{P}_{T2.5C1} / \overline{P}_{T2.5C0}])$
$\% \Delta\overline{P}_{T2.5F1} = 100 \cdot (1 - [\overline{P}_{T2.5F1} / \overline{P}_{T2.5F0}])$
$\% \Delta\overline{P}_{S2.5C1} = 100 \cdot (1 - [\overline{P}_{S2.5C1} / \overline{P}_{S2.5C0}])$
$\% \Delta\overline{P}_{S2.5F1} = 100 \cdot (1 - [\overline{P}_{S2.5F1} / \overline{P}_{S2.5F0}])$
$\% \Delta(\Delta P/P)_{2.5C1} = 100 \cdot (1 - [(\Delta P/P)_{2.5C1} / (\Delta P/P)_{2.5C0}])$
$\% \Delta(\Delta P/P)_{2.5T1} = 100 \cdot (1 - [(\Delta P/P)_{2.5F1} / (\Delta P/P)_{2.5F0}])$
$\% \Delta(\Delta P/P)_{2.5M1} = 100 \cdot (1 - [(\Delta P/P)_{2.5M1} / (\Delta P/P)_{2.5M0}])$

NOTE: @ indicates average over all bosses (α) and immersions (β) shown in range column.

Table 3

Technique 2 – Calculation Procedure Using One Rake in Fan and Core and Two Static Probes for Intermediate Averages

INTERMEDIATE AVERAGE	RANGE OF BOSS AND IMMERSION
$\overline{P}_{T2.5C2} = @(PT25\ -\alpha\ -\beta)$	α = 23 or 113 or 293 β = 1, 2, 3
$\overline{P}_{T2.5F2} = @(PT25F\ -\alpha\ -\beta)$	α = 68 or 248 or 338 β = 1, 2, 3
$\overline{P}_{S2.5C2} = @(PS25\ -\alpha\ -\beta)$	α = 37 or 98 or 278 β = I, 0
$\overline{P}_{S2.5F2} = @(PS25F\ -\alpha\ -\beta)$	α = 84 or 264 or 321 β = I, 0

$$(\Delta P/P)_{2.5C2} = 1 - (\overline{P}_{S2.5C2} / \overline{P}_{T2.5C2})$$

$$(\Delta P/P)_{2.5F2} = 1 - (\overline{P}_{S2.5F2} / \overline{P}_{T2.5F2})$$

$$(\Delta P/P)_{2.5M2} = C_{C2} \cdot (\Delta P/P)_{2.5C2} + C_{F2} \cdot (\Delta P/P)_{2.5F2} + C_{02}$$

} FORMULA

VARIATION FACTORS TO TECHNIQUE 0

$$\% \Delta\overline{P}_{T2.5C2} = 100 \cdot (1 - [\overline{P}_{T2.5C2} / \overline{P}_{T2.5C0}|)$$

$$\% \Delta\overline{P}_{T2.5F2} = 100 \cdot (1 - [\overline{P}_{T2.5F2} / \overline{P}_{T2.5F0}|)$$

$$\% \Delta\overline{P}_{S2.5C2} = 100 \cdot (1 - |\overline{P}_{S2.5C2} / \overline{P}_{S2.5C0}|)$$

$$\% \Delta\overline{P}_{S2.5F2} = 100 \cdot (1 - |\overline{P}_{S2.5F2} / \overline{P}_{S2.5F0}|)$$

$$\% \Delta(\Delta P/P)_{2.5C2} = 100 \cdot (1 - |(\Delta P/P)_{2.5C2} / (\Delta P/P)_{2.5C0}|)$$

$$\% \Delta(\Delta P/P)_{2.5T2} = 100 \cdot (1 - |(\Delta P/P)_{2.5F2} / (\Delta P/P)_{2.5F0}|)$$

$$\% \Delta(\Delta P/P)_{2.5M2} = 100 \cdot (1 - |(\Delta P/P)_{2.5M2} / (\Delta P/P)_{2.5M0}|)$$

NOTE: @ indicates average over all bosses (α) and immersions (β) shown in range column.

Table 4

Technique 3 – Calculation Procedure Using Centered Total Probe in Core and Fan and O.D. Static Probe for Intermediate Average

INTERMEDIATE AVERAGE	RANGE OF BOSS AND IMMERSION
$\bar{P}_{T2.5C3} = @(PT25\ -\alpha\ -\beta)$	α = 23 or 113 or 293 β = 2
$\bar{P}_{T2.5F3} = @(PT25F\ -\alpha\ -\beta)$	α = 68 or 248 or 338 β = 2
$\bar{P}_{S2.5C3} = @(PS25\ -\alpha\ -\beta)$	α = 37 or 98 or 278 β = 0
$\bar{P}_{S2.5F3} = @(PS25F\ -\alpha\ -\beta)$	α = 84 or 264 or 321 β = 0

$$(\Delta P/P)_{2.5C3} = 1 - (\bar{P}_{S2.5C3} / \bar{P}_{T2.5C3})$$

$$(\Delta P/P)_{2.5F3} = 1 - (\bar{P}_{S2.5F3} / \bar{P}_{T2.5F3})$$

$$(\Delta P/P)_{2.5M3} = C_{C3} \cdot (\Delta P/P)_{2.5C3} + C_{F3} \cdot (\Delta P/P)_{2.5F3} + C_{03}$$

} FORMULA

VARIATION FACTORS TO TECHNIQUE 0
$\% \Delta\bar{P}_{T2.5C3} = 100 \cdot (1 - [\bar{P}_{T2.5C3} / \bar{P}_{T2.5C0}])$
$\% \Delta\bar{P}_{T2.5F3} = 100 \cdot (1 - [\bar{P}_{T2.5F3} / \bar{P}_{T2.5F0}])$
$\% \Delta\bar{P}_{S2.5C3} = 100 \cdot (1 - [\bar{P}_{S2.5C3} / \bar{P}_{S2.5C0}])$
$\% \Delta\bar{P}_{S2.5F3} = 100 \cdot (1 - [\bar{P}_{S2.5F3} / \bar{P}_{S2.5F0}])$
$\% \Delta(\Delta P/P)_{2.5C3} = 100 \cdot (1 - [(\Delta P/P)_{2.5C3} / (\Delta P/P)_{2.5C0}])$
$\% \Delta(\Delta P/P)_{2.5T3} = 100 \cdot (1 - [(\Delta P/P)_{2.5F3} / (\Delta P/P)_{2.5F0}])$
$\% \Delta(\Delta P/P)_{2.5M3} = 100 \cdot (1 - [(\Delta P/P)_{2.5M3} / (\Delta P/P)_{2.5M0}])$

NOTE: @ indicates average over all bosses (α) and immersions (β) shown in range column.

Table 5 summarizes the specific rakes/probes used for each of the three alternative techniques. Each of the $(\Delta P/P)_{2.5m}$ values from techniques 1, 2, and 3 were compared to the average of all measurements. However, prior to discussing these results, it is necessary to establish the operating conditions tested as well as the validity and consistency of the fan operating obtained at these operating conditions.

Figure 2 shows the fan operating line for five flight conditions tested (see Figure 3.1). Figure 2 shows that a reasonably consistent fan operating line was obtained with a nominal jet area and a nominal fan exit $(\Delta P/P)_{2.5m} = 0.158$. Other engine match parameters such as speed-flow relationships, FTIT vs. N2 and N1 vs. N2 relationships, also verified that the points selected were valid for the desired $(\Delta P/P)_{2.5m}$ evaluation.

Figure 3 presents the correct average (Technique 0) $(\Delta P/P)_{2.5m}$ data for the selected points previously shown on the fan map. Figure 4 shows these data corrected to nominal jet area and plotted against their scheduled values. This figure shows that the XD11 fan exit Mach number was, in general, higher than the current schedule and that a constant $(\Delta P/P)_{2.5m}$ adjustment of 0.045 will provide a reasonable fit ($\pm$10%) to the data collected at all flight conditions. Referring to the inset in Figure 1, it can be seen that a 10% error in measured $(\Delta P/P)_{2.5m}$ will result in only a 5% error in fan pressure ratio at constant corrected airflow. That is, at intermediate power, a 10% error in $(\Delta P/P)_{2.5m}$ yields a 0.15 error in fan pressure ratio, while at idle, the fan pressure ratio error is 0.05. These operating tolerances are within those using the new $(\Delta P/P)_{2.5m}$ schedule shown in Figure 4, the MVCS logic will provide a fan operating line within the BOM operating line limits shown in Figure 2 for the flight conditions tested. This schedule simply requires a bias adjustment of 0.045 to the current schedule.

Table 5

XD-11 ΔP/P SENSOR DATA

SENSOR		TECHNIQUE 1	TECHNIQUE 2	TECHNIQUE 3
$P_{T2.5C}$:	22-1			
	22-2			
	22-3			
	113-1	X	X	
	113-2	X	X	X
	113-3	X	X	
	293-1	X		
	293-2	X		
	293-3	X		
$P_{S2.5C}$:	37-OD	X		
	37-ID	X		
	98-OD	X	X	X
	98-ID	X		
	278-OD	X		
	278-ID	X		
$P_{T2.5F}$:	68-1	X		
	68-2	X		X
	68-3	X		
	248-1	X	X	
	248-2	X	X	
	248-3	X	X	
	338-1			
	338-2			
	338-3			
$P_{S2.5F}$:	84-OD	X		
	84-ID	X		
	264-OD	X	X	X
	264-ID	X	X	
	321-OD	X		
	321-ID	X		

NOTE: XXX-YY is boss at XXX degrees with immersion YY

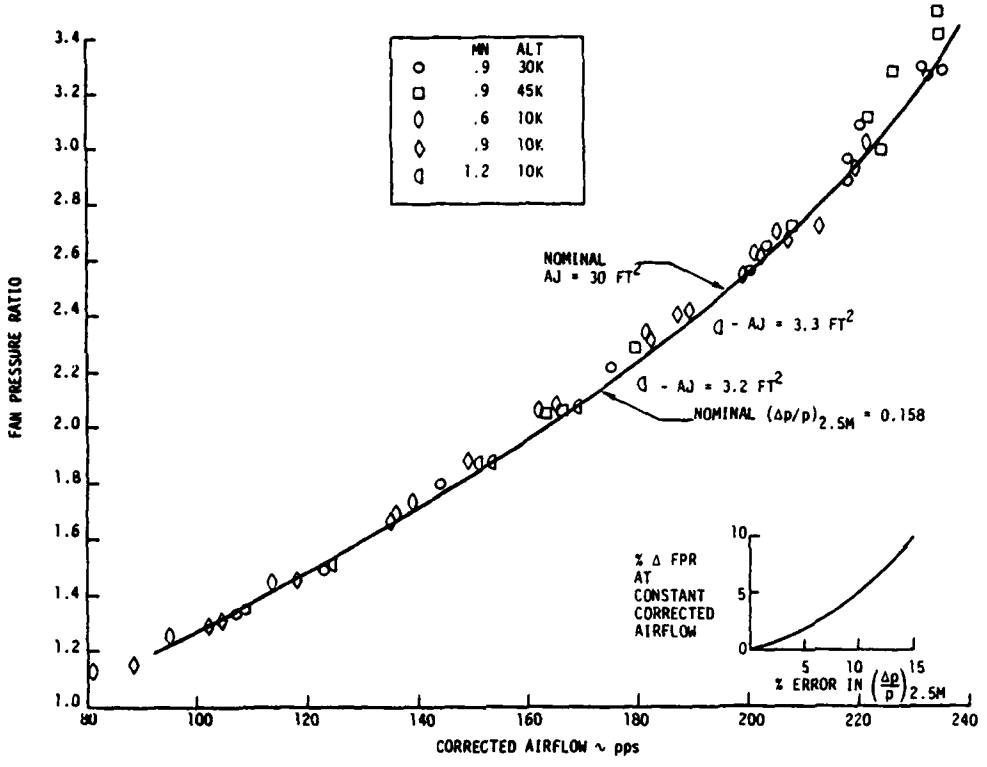

Figure 2 Fan Operating Line for XD-11 at Subsonic Test Points

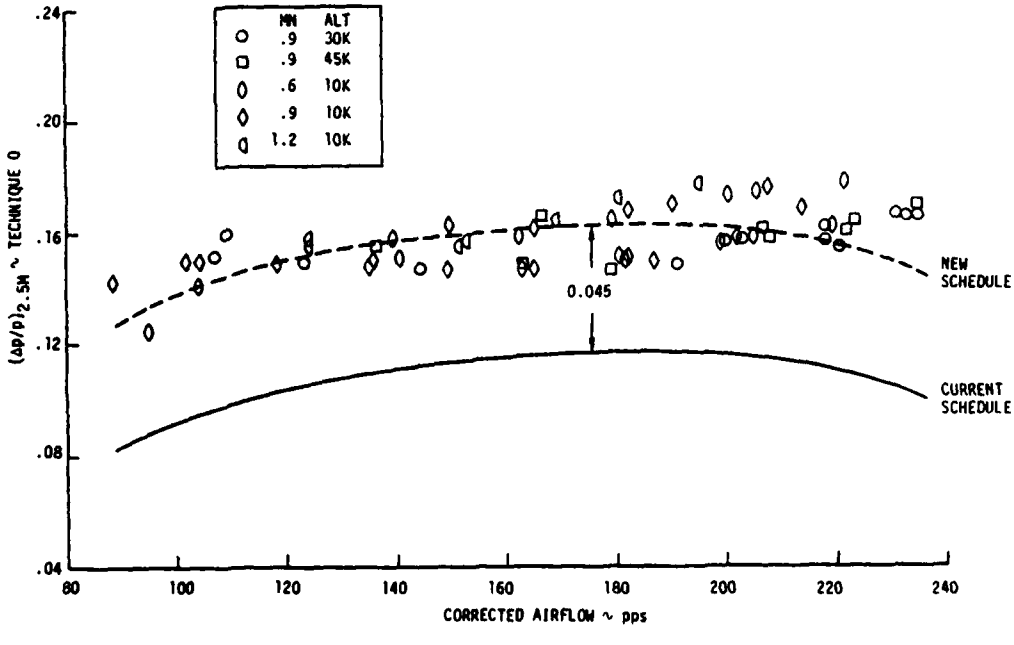

Figure 3 Comparison of Scheduled (ΔP/P) to Technique 0 (ΔP/P) As a Function of Fan Corrected Airflow at Subsonic Test Points

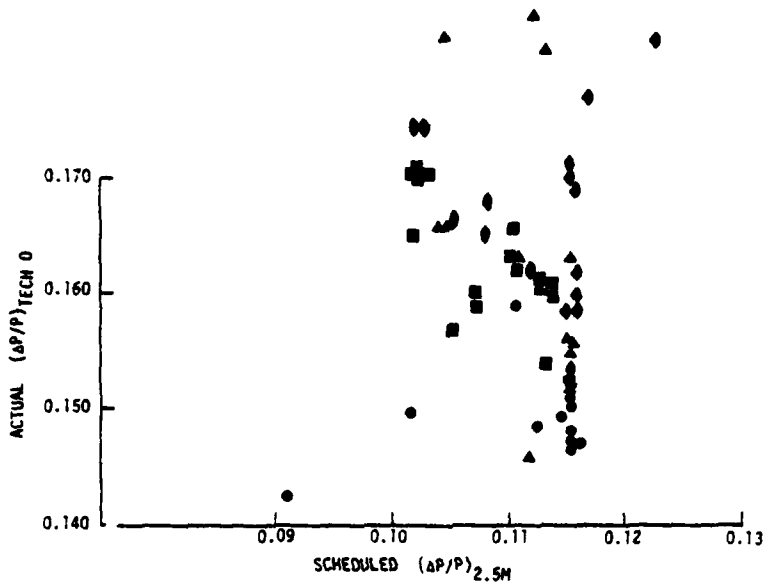

Figure 4(a) Comparison of Scheduled (ΔP/P) and Technique 0 (ΔP/P) at Subsonic Test Points

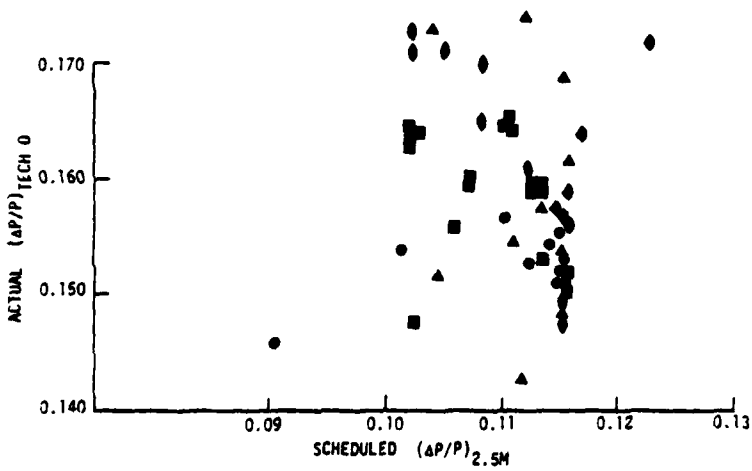

Figure 4(b) Comparison of Scheduled (ΔP/P) and Technique 0 (ΔP/P) Corrected for Off-Nominal Nozzle Area

Figure 5 shows the comparison of techniques 1, 2, and 3 to technique 0 in terms of percentage error in $(\Delta P/P)_{2.5\ m}$ for each technique. This figure shows that for particular flight conditions and specific power settings, more accuracy is obtained with more probes. However, even the minimum number of probes (technique 3) yields acceptable predictability of $(\frac{\Delta P}{P})_{2.5m}$. Consequently, due to its simplicity, the remainder of this analysis will concentrate on how technique 3 can be used to synthesize $(\Delta P/P)_{2.5m}$ and how accurate that calculation might be.

Figure 6 is the comparison of $(\Delta P/P)_{2.5m}$ using technique 3 to the current MVCS schedule. This figure shows that a similar positive bias (0.045) would tend to make the schedule fit the XD11 data better. However, these data also show some skewness relative to the new schedule which was not evidenced in the technique 0 data (Figure 2). This skewness is derived from the fact that the reduced number of sensors cannot properly accommodate fan exit profile shifts at all flight conditions or power settings. Therefore, a technique must be developed for adjusting the technique 3 data of Figure 6 so that it can be presented to the control in a form that emulates technique 0 at all airflow settings (fan operating points). The capability for this already exists in the MVCS software. However, prior to deriving these relationships it is interesting to compare the scatter of the XD11 engine data using technique 3 to the scatter obtained for $(\Delta P.P)_{2.5m}$ from the F100 simulation (CCD 1103-2.0) during the MVCS Phase I design effort.

Figure 7 shows the $(\Delta P/P)_{2.5m}$ data from both the engine tests on XD11 and from the F100 simulation at a range of flight conditions. It can be seen that the scatter bands for these two data sets are quite comparable.

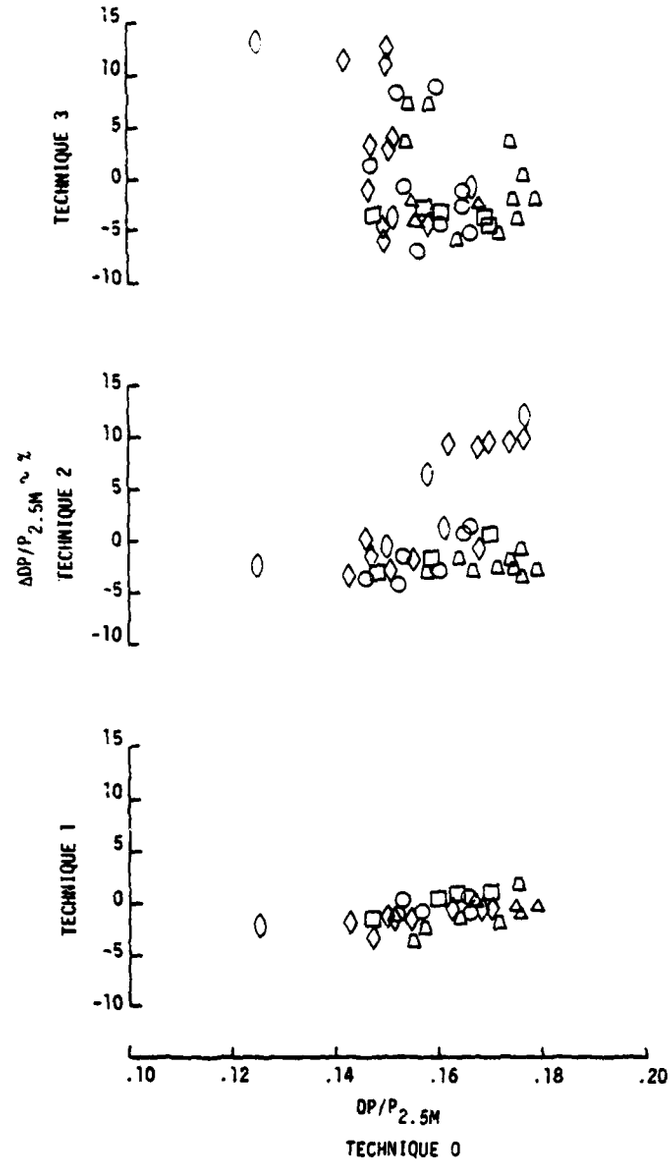

Figure 5 Comparison of Techniques 1, 2, and 3 Calculation Procedures to Technique 0

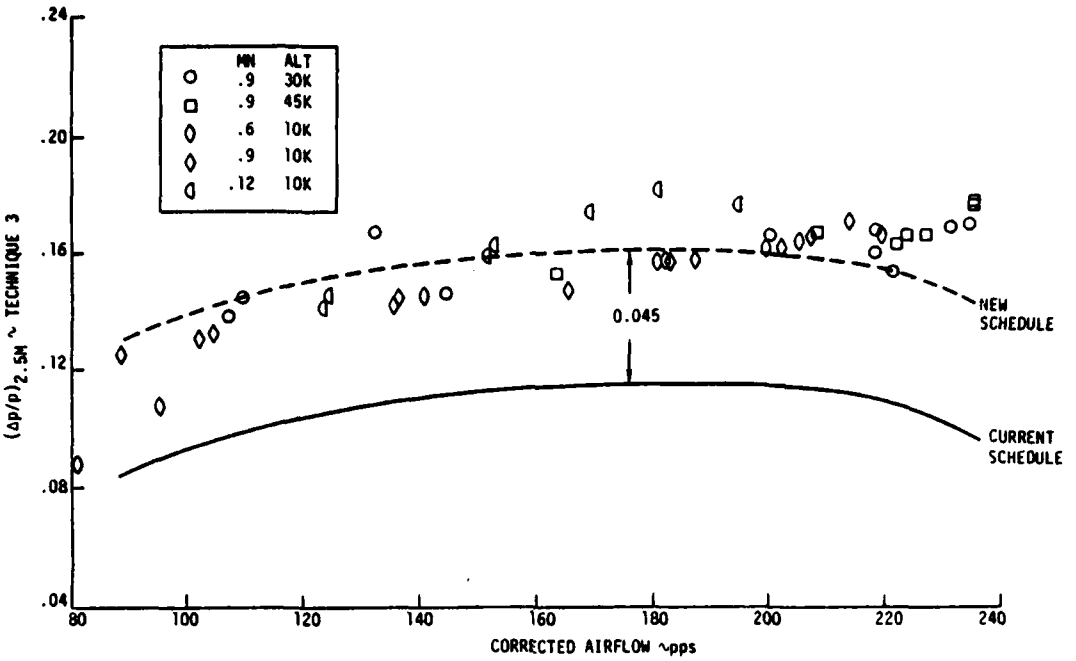

Figure 6 Comparison of Technique 3 ($\Delta P/P$) Calculation to Schedule

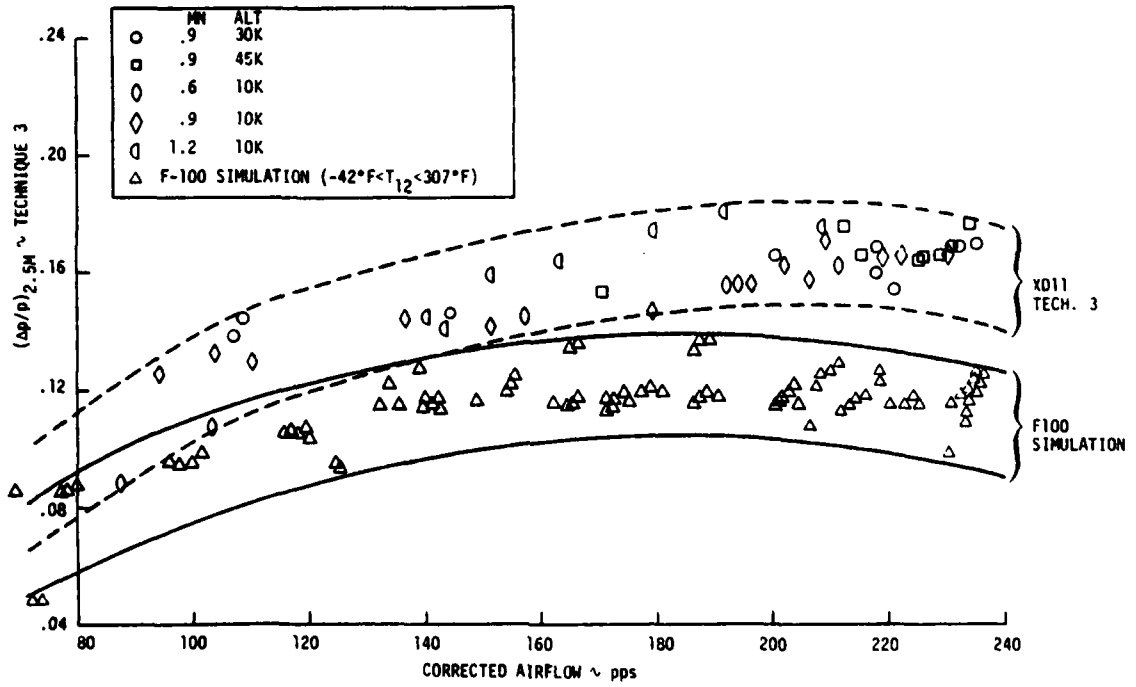

Figure 7 Comparison of Technique 3 ($\Delta P/P$) to Data Generated with F100 Dynamic Calculation Used to Generate MVCS Schedule (Subsonic Points)

In summary, it has been shown thus far that:

(1) A consistent fan operating line was obtained at the five flight conditions tested.

(2) The $(\Delta P/P)_{2.5m}$ data from XD11 was offset from the current schedule by a constant bias (0.045) if technique 0 "correct" average data was used.

(3) That technique 3 offered just as viable an alternative as techniques 1 and 2.

(4) That the XD11 $(\Delta P/P)_{2.5m}$ data was no worse than predicted from the F100 simulation.

What remains to be shown is how the technique 3 data will be adjusted to offset the measured slope change relative to technique 0 and what the magnitude of errors (mean and two sigma) in these two techniques were. Table 6 summarizes the mean and two sigma errors for these two techniques as a function of PLA and corrected airflow. The PLA values are approximate for various flight conditions. This table shows that the mean $(\Delta P/P)_{2.5m}$ is a constantly increasing function as corrected airflow increases from 105 pps to 225 pps regardless of which technique is used to calculate it. The table also shows that the two-sigma values were quite small (0.010 to 0.040) over the full range of fan operating points. The data from Table 6 for technique 0 are plotted in Figure 8 to illustrate the meaning of the variations calculated.

Table 6

$(\Delta P/P)_{2.5m}$ Data Comparison

APPROXIMATE PLA	AIRFLOW (pps)	TECHNIQUE 0	TECHNIQUE 3
83°	225	.163 $\pm$ .012*	.167 $\pm$ .010*
75°	200	.160 $\pm$ .024	.164 $\pm$ .018
65°	175	.156 $\pm$ .018	.159 $\pm$ .024
40°	145	.153 $\pm$ .014	.147 $\pm$ .012
24°	105	.143 $\pm$ .036	.127 $\pm$ .040

* mean $\pm$ 2σ

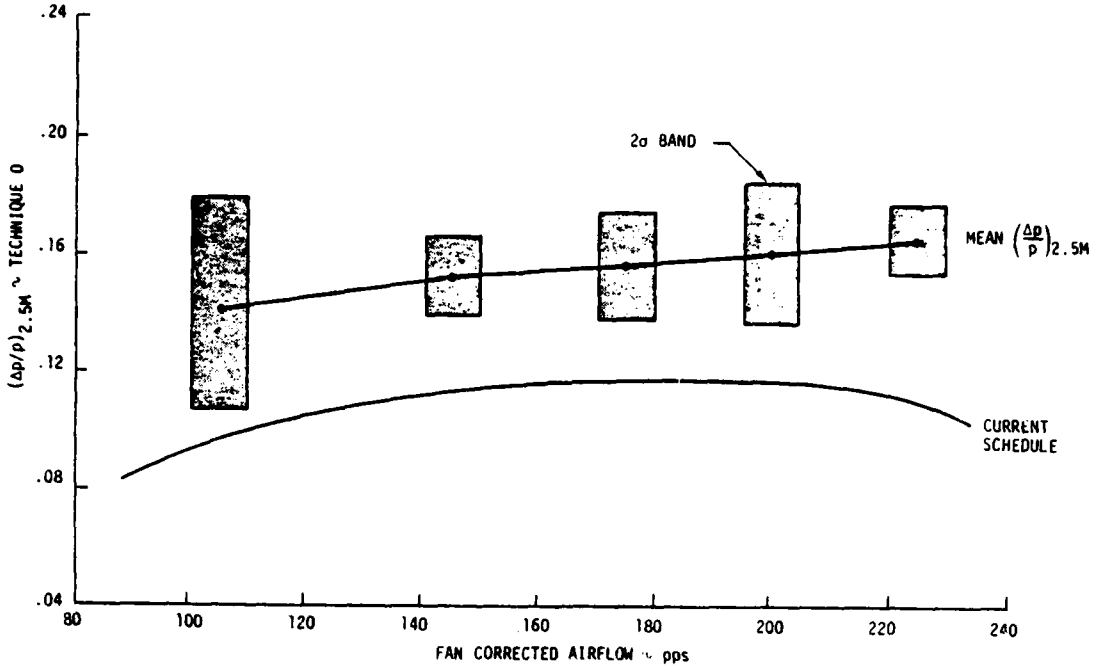

Figure 8 Illustration of 2σ Uncertainty about Mean Technique (ΔP/P) Data As a Function of Fan Airflow

Figure 9 shows the mean values of $(\Delta P/P)_{2.5m}$ for techniques 0 and 3 vs. the current schedule. This figure again illustrates the skewness in technique 3 which was previously noted in Figures 6 and 7. It should be noted, however, that the skewness is small on the average and that it is well within the documented data scatter as shown in Figures 4 and 6. Also, the skewness is much less than the two-sigma scatter bands calculated for the same data (Figure 8). Nevertheless, it is more correct to utilize the software capability to adjust the technique 3 data as accurately as possible. This will in effect eliminate another small source of error and thereby eliminate fan operating line offset during MVCS testing. Therefore, the calculation format shown in Table 4 was utilized to obtain a "modified" technique 3 equation. All of the data collected at the five flight conditions were analyzed to obtain weighting factors which would cause the

modified technique 3 to match the "correct" average. The equation obtained was:

$$\left[\left(\frac{\Delta P}{P}\right)_{2.5m}\right]_{MODIFIED} = 0.46445 \left(\frac{\Delta P}{P}\right)_{2.5m} = 0.56825 \left(\frac{\Delta P}{P}\right)_{2.5m} + 0.0$$

where

$C_{C3} = 0.46445$

$C_{F3} = 0.56825$

$C_{03} = 0.0$

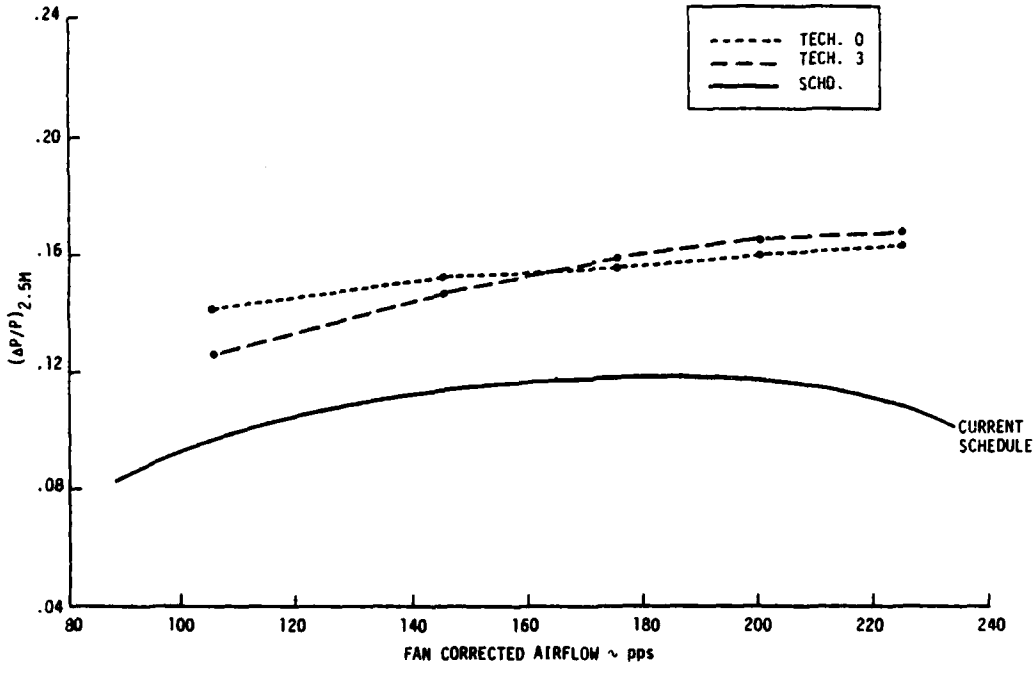

Figure 9 Comparison of Techniques 3 and 0 Mean Lines with Respect to MVCS Schedule

This equation was then applied to all the data collected to assess its accuracy. Figure 10 shows a plot of the modified technique 3 vs. technique 0. It can be seen that this technique

will provide satisfactory results for all flight conditions simulated during the BOM testing.

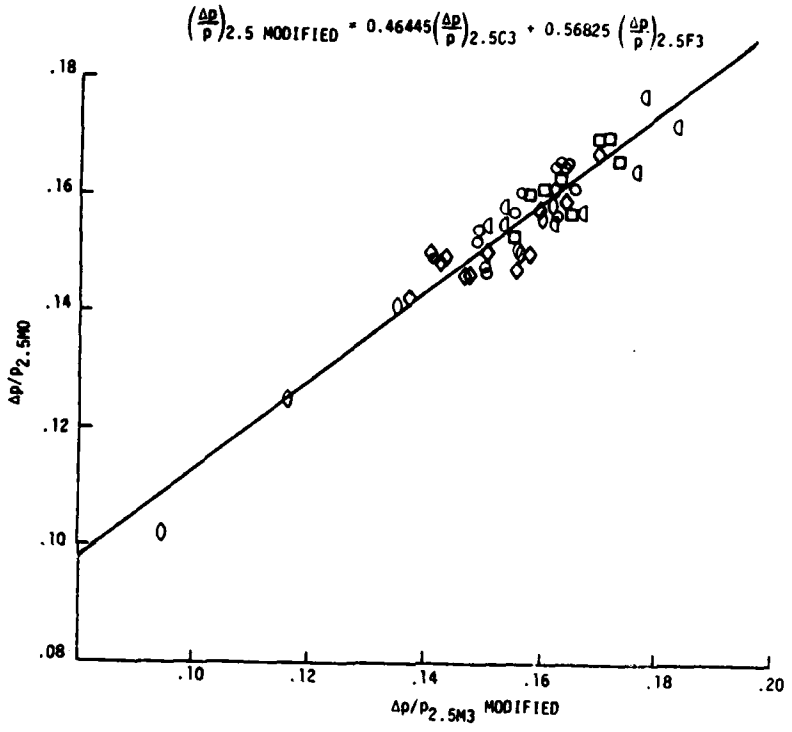

Figure 10 Comparison of Modified Technique 3 Calculation Procedure with Actual Technique 0 ($\Delta P/P$)

☆U.S.Government Printing Office: 1980 — 657-084/149

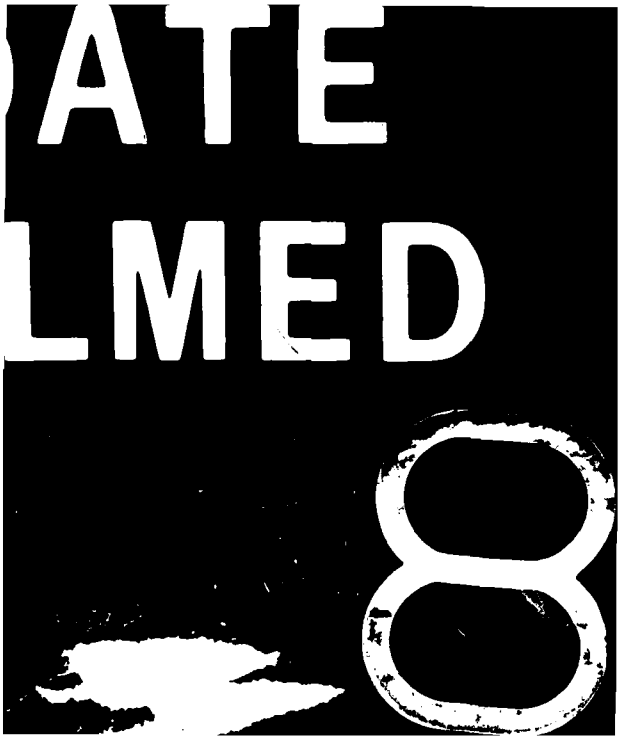
ATE
LMED
8